# EFFECT OF HOT PRESSING TEMPERATURE ON THE ELECTROCHEMICAL STABILITY OF LI<sub>2</sub>S-P<sub>2</sub>S<sub>5</sub> (75 - 25 % MOLE) AS A SOLID ELECTROLYTE

By

Maria Regina Garcia Mendez

#### A THESIS

Submitted to
Michigan State University
in partial fulfillment of the requirements
for the degree of

Materials Science and Engineering-Master of Science

2015

#### **ABSTRACT**

# EFFECT OF HOT PRESSING TEMPERATURE ON THE ELECTROCHEMICAL STABILITY OF LI<sub>2</sub>S-P<sub>2</sub>S<sub>5</sub> (75 – 25 % MOLE) AS A SOLID ELECTROLYTE

By

#### Maria Regina Garcia Mendez

Solid state batteries can contribute to a more sustainable energy future providing the energy required when needed. It can facilitate the integration of renewable energy into the electrical grid and can provide the energy density redequir to make electric vehicles a massive technology without greenhouse emissions in operating conditions. To concretize the latter, high-performance electrolytes are necessary. Li<sub>2</sub>S-P<sub>2</sub>S<sub>5</sub> (75-25% mole) is a promising solid-electrolyte that could potentially be used for this purpose. Its most appealing features include: high ionic conductivity at room temperature (~10<sup>-3</sup> S/cm), low-temperature processing conditions, and low cost. Most likely, Li<sub>2</sub>S-P<sub>2</sub>S<sub>5</sub> (75-25% mole) would be integrated in a battery system using Li metal as an anode. Therefore, its stability against metallic lithium must be understood. The purpose of this work is to characterize the effect of Li<sub>2</sub>S-P<sub>2</sub>S<sub>5</sub> (75-25% mole) processing conditions, most specifically hot pressing, and their effect on Li stability. It was found that improvements on electrochemical performance can be attained by promoting particle chemistry during hot pressing.

#### **ACKNOWLEDGEMENTS**

I would like to express my sincere gratitude and appreciation to my advisor Dr. Jeff Sakamoto for transcending in his role. His passion for science, immense curiosity, patience and kindness makes him an outstanding professor. I would like to thank him for encouraging me to challenge myself and always do better.

I would like to thank Fulbright for giving me the opportunity to gain knowledge in the field I wanted to be part of; Materials Science and Engineering, and the countless benefits this experience has brought to me.

I would like to thank my committee members Dr. Donald Morelli and Dr. Carl Boehlert for agreeing to be part of my committee and for their great disposition to help me throughout my studies at Michigan State University. I would also like to thank Dr. Morelli for granting me access to his laboratory when needed. Additionally, I would like to acknowledge the collaboration and excellent teamwork of Dr. Fuminori Mizuno, Dr. Tim Arthur, Dr. Ruigang Zhang and Dr. Paul Fanson of Toyota Motor Engineering & Manufacturing North America, Inc. for Scanning Electron Microscopy (SEM), Differential Scanning Calorimetry (DSC) and X-Ray Diffraction (XRD) Analyses.

I want to thank each of the members of the laboratory that have made this experience more meaningful and enjoyable: Dena Shahriari, Yunsung Kim, Asma Sharafi, Travis Thompson, Dan Lynam, Isabel David and Young-Sam Park. Finally, I would like to thank my family and closest friends that have unconditionally supported me and encouraged me throughout my life.

## TABLE OF CONTENTS

LIST OF TA	ABLES	vi
LIST OF FI	GURES	vii
1. Introdu	ction	1
1.1 En	ergy demand and storage need	1
1.2 Ele	ectrochemical energy storage devices	2
1.3 Ne	ed for solid state electrolytes	6
1.4 Inc	organic solid state Li-ion conductors	8
1.4.1	Crystalline ceramic electrolytes	9
1.4.1.1	Perovskite	9
1.4.1.2	NASICON-Type	9
1.4.1.3	LISICON and thio-LISICON Type	10
1.4.1.4	Garnet	10
1.4.2	Inorganic non-crystalline solid electrolytes	11
1.4.2.1	LIPON	11
1.4.2.2	Sulfide glasses	11
1.4.2.3	Li <sub>2</sub> S-P <sub>2</sub> S <sub>5</sub>	12
1.5 Ce:	ramic electrolyte processing and characterization techniques	14
1.5.1	Planetary ball milling	14
1.5.2	Densification of sulfide electrolytes	16
1.5.3	Electrochemical characterization	21
1.5.3.1	Electrochemical Impedance Spectroscopy (EIS)	21
1.5.3.2	Preconditioning	
1.5.3.3	DC asymmetric polarization method	25
1.6 Ma	terials characterization techniques	26
1.6.1	X-Ray Diffraction (XRD)	26
1.6.2	Differential Scanning Calorimetry (DSC)	26
1.6.3	Scanning Electron Microscopy (SEM)	27
2. The effe	ect of hot pressing temperature on the electrochemical stability of Li <sub>2</sub> S-P <sub>2</sub> S <sub>5</sub> (	(75 - 25)
	1 0 1	
2.1. Int	roduction	28
	sults and Discussion	
2.2.1.	Evaluating the effect of hot pressing temperature on LPS bulk properties	
2.2.1.1.		
2.2.1.2.		
2.2.2.	Evaluating the chemical and electrochemical stability of LPS	
2.2.2.1.		

2.2.2.2. Cross-sectional analysis	46
2.2.3. Materials characterization	48
2.2.3.1. X-Ray Diffraction Analysis	48
2.2.3.2. Differential Scanning Calorimetry	50
2.2.3.3. Scanning Electron Microscopy (SEM) and Energy Dispersive Spectrometry	
(EDS)	52
2.3. Conclusion	53
2.4. Future directions	54
REFERENCES	55

## LIST OF TABLES

Table 1. Capacitance values and their possible interpretation (Irvine et al. 1990)	.23
Table 2. 75Li <sub>2</sub> S-25P <sub>2</sub> S <sub>5</sub> hot pressed pellets (12.7mm in diameter) between 130°C and 190°C for electrochemical performance analysis– Data set no.1	
Table 3. 75Li <sub>2</sub> S-25P <sub>2</sub> S <sub>5</sub> hot pressed pellets (12.7mm in daiameter) between 130°C and 190°C for materials characterization— Data set no.2	
Table 4. Li/LPS/Li cell preconditioning at room temperature	.37
Table 5. Cross-sectional analysis on cold-pressed and hot-pressed pellets between 130°C and 150°C	.46
Table 6. Cross-sectional analysis on cold-pressed and hot-pressed pellets between 160°C and 190°C	.47

## LIST OF FIGURES

Figure 1. Shares of world primary energy (Chu 2012)
Figure 2. Ragone plot for various energy devices (Wachsman et al. 2011)3
Figure 3. Schematic of a lithium ion battery (LIB) (Dunn et al. 2011)6
Figure 4. Amount of H <sub>2</sub> S generated from pelletized Li <sub>2</sub> S-P <sub>2</sub> S <sub>5</sub> (LPS) glasses with different Li <sub>2</sub> S contents (Muramatsu et al. 2011)
Figure 5. Schematic of specific volume changes observed as a glass is heated through Tg (Callister 2007)
Figure 6. a) Densification pressure dependence of 75Li <sub>2</sub> S-25P <sub>2</sub> S <sub>5</sub> (mol%) glass solid electrolyte, b) SEM image of 75Li <sub>2</sub> S-25P <sub>2</sub> S <sub>5</sub> glass powder. SEM images of fracture cross-sections of 75Li <sub>2</sub> S-25P <sub>2</sub> S <sub>5</sub> glass powders pressed at c) 74 and d) 360MPa (Sakuda et al. 2013)
Figure 7. Photographs of the pellets of the $80\text{Li}_2\text{S}-20\text{P}_2\text{S}_5$ sample pressed at a) room temperature, b) $180^{\circ}\text{C}$ , c) $210^{\circ}\text{C}$ and d) $240^{\circ}\text{C}$ for 2h, and e) $210^{\circ}\text{C}$ for 4h (Kitaura et al. 2011)19
Figure 8. Young's modulus of $xLi_2S*(100-x)P_2S_5$ (mol%) glass pellets prepared by hot press and cold press at 360 MPa (Sakuda et al. 2013)
Figure 9. Schematic of a double acting die configuration21
Figure 10. Experimental arrangement generally used for variable frequency AC measurements to evaluate ionic transport in a solid electrolyte
Figure 11. Schematic complex plane plot of the Debye equivalent circuit (Huggins, 2009)23
Figure 12. Schematic of the pressure and temperature profiles followed during hot pressing tests
Figure 13. Fractured surfaces of hot-pressed samples between 130°C and 170°C33
Figure 14. DSC spectra of Li <sub>2</sub> S-P <sub>2</sub> S <sub>5</sub> (75 – 25 % mole) powder as prepared34
Figure 15. Effect of hot pressing at 130 and 140°C on DSC spectra of 75Li <sub>2</sub> S-25P <sub>2</sub> S <sub>5</sub> 35
Figure 16. Li/75Li <sub>2</sub> S-25P <sub>2</sub> S <sub>5</sub> /Li cell preconditioning at room temperature, 0.01 mA/cm <sup>2</sup> 36

Figure 17. Nyquist plot of Li/LPS/Li cell before preconditioning at room temperature - Cold-pressed pellet
Figure 18. Nyquist plot of Li/LPS/Li cell before preconditioning at room temperature -Hot-pressed samples
Figure 19. Nyquist plot of Li/LPS/Li cell after preconditioning at room temperature - Cold-pressed pellet
Figure 20. Nyquist plot of Li/LPS/Li cell after preconditioning at room temperature -Hot-pressed samples
Figure 21. 75Li <sub>2</sub> S-25P <sub>2</sub> S <sub>5</sub> resistance (normalized by its aspect ratio) after preconditioning42
Figure 22. DC asymmetric polarization test at room temperature
Figure 23. Total charge passed through Li/75Li <sub>2</sub> S-25P <sub>2</sub> S <sub>5</sub> /Li cell before significant drop in potential is observed in DC asymmetric polarization test
Figure 24. Nyquist plot of Li/LPS/Li cell after DC asymmetric polarization at room temperature – Hot-pressed pellets at 180°C and 190°C
Figure 25. Cross-sectional analysis on cold-pressed and hot-pressed pellets between 130°C and 150°C
Figure 26. Cross-sectional analysis on cold-pressed and hot-pressed pellets between 160°C and 190°C
Figure 27. Effect of hot pressing temperature on 75Li <sub>2</sub> S-25P <sub>2</sub> S <sub>5</sub> structure
Figure 28. Effect of DC cycling on 75Li <sub>2</sub> S-25P <sub>2</sub> S <sub>5</sub> structure (hot pressed at 190°C)50
Figure 29. Effect of hot pressing and Li cycling on DSC spectra of 75Li <sub>2</sub> S-25P <sub>2</sub> S <sub>5</sub> hot-pressed at 130°C
Figure 30. Effect of hot pressing and Li cycling on DSC spectra of 75Li <sub>2</sub> S-25P <sub>2</sub> S <sub>5</sub> hot-pressed at 140°C
Figure 31. Fractured surfaces of hot pressed and DC cycled 75Li <sub>2</sub> S-25P <sub>2</sub> S <sub>5</sub> pellets53

#### 1. Introduction

#### 1.1 Energy demand and storage need

The world's energy demand will increase from approximately 12 billion metric tons of oil equivalents (t.o.e) in 2009 to 18 billion t.o.e by 2035. The International Energy Agency (IEA) projects that the carbon dioxide emissions are expected to increase from 29 metric gigatons per year (Gt/yr) to between 36 and 43 Gt/yr. (Lee, 2011). The world's dependence on fossil fuels to produce energy is unprecedented taking into account it comprises roughly 86% of the world's main energy consumption (Figure 1, Chu, 2012). Furthermore, according to the Intergovernmental Panel on Climate Change (IPCC) 2014 report, carbon dioxide emissions from fossil fuel combustion and industrial processes contributed about 78% of the total greenhouse gases emission increase for the past 40 years. Thus, the need of renewable sources of energy is of great relevance to obtain a sustainable and secure energy future. Developed countries have started to employ diverse strategies to decrease the fossil fuel dependence as the development of electric vehicles, increased deployment of renewable energy sources, and also an integration of electrical energy transmission, distribution, and storage for the electrical grid. (Dunn 2011; Chu 2012).

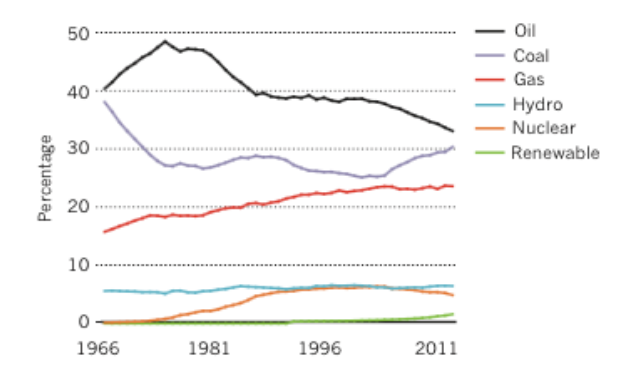


Figure 1. Shares of world primary energy (Chu 2012)

Underlying these strategies is the recognition that inexpensive and reliable energy is vital for economic development. Electrical Energy Storage (EES) cannot possibly address all of these challenges. However, EES does offer a well-established approach for improving grid reliability and utilization. Whereas transmission and distribution systems are responsible for moving electrical power to end users, the EES systems provide uninterrupted service (Dunn et al. 2011). The energy storage technologies available for large-scale applications can be divided into four types: mechanical, electrical, chemical and electrochemical. This work will focus on electrochemical energy storage, due to its desirable features including pollution-free operation, flexible power and energy characteristics to meet small, medium or large-scale applications as well as reliability (Dunn et al. 2011). The application of interest in this work will be electric vehicles (EV).

The important metrics to evaluate EES to enable vehicle electrification include: specific power that refers to the amount of power per unit mass of the rate at which energy is extracted from a battery and specific energy that refers to the amount of energy per unit mass of the battery. This translates in vehicles as follows: higher specific energy will enable a vehicle to travel farthest distances without being recharged; meanwhile the specific power refers to vehicle acceleration and charge rate. Thus, the most important characteristics for an EV EES device are: specific power, energy density, lifetime, cost and maintenance. (Chu, 2007)

#### 1.2 Electrochemical energy storage devices

Current EES devices will not meet future energy storage requirements. (Chu, 2007). Therefore, the performance of state-of-the-art electrochemical devices has to be addressed considering the challenges that each needs to overcome for electric vehicles (EVs) or plug-in hybrid vehicles (PHEVs).

Supercapacitors, solid oxide fuel cells (SOFCs) and batteries are going to be discussed since all three can be charged under a few hours as seen from the diagonal dotted lines in the Ragone plot (Figure 2).

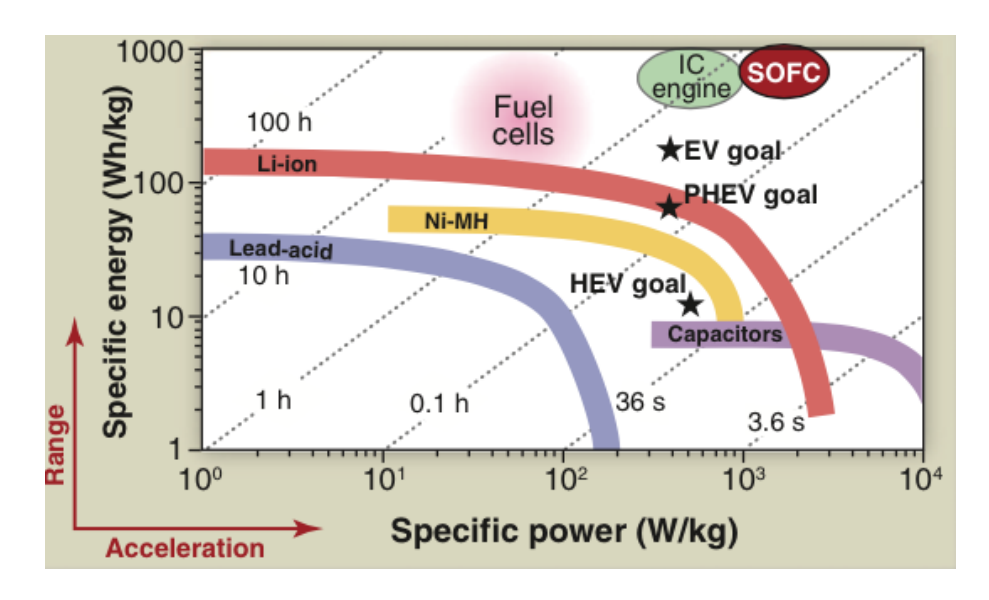


Figure 2. Ragone plot for various energy devices (Wachsman et al. 2011)

Supercapacitors store energy by physically separating positive and negative charges, which are stored on two parallel plates divided by an insulator. These devices have a number of potentially high-impact characteristics, such as fast charging (within seconds), reliability and wide operating temperatures (Chu, 2007). Since there are no chemical variations on the electrodes these devices have a long cycle life (hundreds of thousands charge-discharge cycles), but low energy density compared to batteries (figure 2) (Khaligh, 2010; Wachsman et al. 2011). Supercapacitors fulfill the power density required for the HEV, PHEV and EV applications, but not the energy density of either. In hybrid electric vehicles (HEV) applications, both batteries and supercapacitors could be combined to maximize the benefits of both components. (Khaligh, 2010)

A SOFC consists of two electrodes (cathode and anode) separated by a solid oxygen ion-

conducting electrolyte. At the cathode, oxygen that comes from air is reduced and the oxygen ions are transported through the electrolyte lattice to the anode where they react with gaseous fuel, yielding heat, water, and carbon dioxide when using hydrocarbon fuels and releasing electrons to the external circuit. (Wachsman, 2011) Multiple cells are combined in series that provide both electrical contacts and gas channels between individual cells. The resulting "stacks" are then arranged in series and parallel configurations to provide the desired voltage and power outputs from portable power and transportation applications to distributed generation and large-scale power generation. This energy storage technology has a high power density, higher than supercapacitors and batteries (figure 2), high conversion efficiency of fuel to electrical energy and waste heat recoverability. However, its main drawback is high operating temperature (about 800°C) limiting the types of materials that can be selected for their fabrication and also leading to a costly technology. (Wachsman, 2011; Khaligh, 2010) Even though SOFCs possess a high power density they have a significant lag due to gas flow rates and require several seconds to respond to a demand that sweeps from 10 to 90% of the total power, affecting vehicles when accelerating (Chu, 2007).

A battery is composed of several electrochemical cells that are connected in series and/or in parallel in order to provide the required voltage and capacity, respectively. Each cell is composed of a positive and a negative electrode, which are where the redox reactions take place. The electrodes are separated by an electrolyte that is a good ionic conductor but a poor electronic conductor (<10<sup>-12</sup> S/cm) to prevent self-discharge of the battery (Nazri et al. 2003). When an external circuit connects the electrodes, the electrons from the anode flow spontaneously to the cathode. The driving force for this reaction is the difference in the chemical potential between electrodes. Simultaneously, a flow of ions goes through the electrolyte in order to decrease the

potential difference caused by the flow of electrons and maintain charge neutrality within the system. (Dunn et al. 2011)

There are several battery chemistries, most of which have been based on aqueous electrolytes. Regardless of their chemistry, batteries store energy within the electrode structure through charge transfer reactions. (Dunn et al. 2011) The lead-acid battery, standard for automobile starting systems, has relatively low energy density, moderate power rate, but low cost, which is the reason why it is still used despite of its drawbacks: lead toxicity and relatively low specific energy. Nickel-Cadmium batteries are more expensive than the lead-acid batteries, have higher energy density and significantly higher power density than lead-acid technology. However, its most significant drawback is Cadmium toxicity, and its potential environmental damage related to cadmium uptake into the soil (Kurzweil 2009). To address the environmental issues with the Ni-Cd battery, gaseous hydrogen in titanium-based alloys have been used in place of cadmium as the negative electrode. This battery technology is known as the Nickel-metal hydride (NMH) battery. (Kurzweil 2009) The NMH battery has a relatively low voltage, moderate energy density, high power density, but nickel is difficult to extract, thus unsustainable and toxic.

Lithium-ion batteries employ non-aqueous electrolytes and use Li-intercalation compounds as electrodes. It offers a high energy density, power rate, cycle life, but it is costly and also uses relatively expensive elements (cobalt) in most Li-ion cathodes. Manganese and iron have been suggested as alternatives to replace cobalt, which are abundant and sustainable (Armand, 2008) Li-ion battery (LIB) technology (Figure 3) is the current leading candidate to meet the near and medium-term needs for hybrid electric vehicles (HEVs) as well as plug-in hybrids (PHEVs), provided that improvements can be achieved in terms of performance, cost, and safety. (Sakamoto, 2012, Armand, 2008).

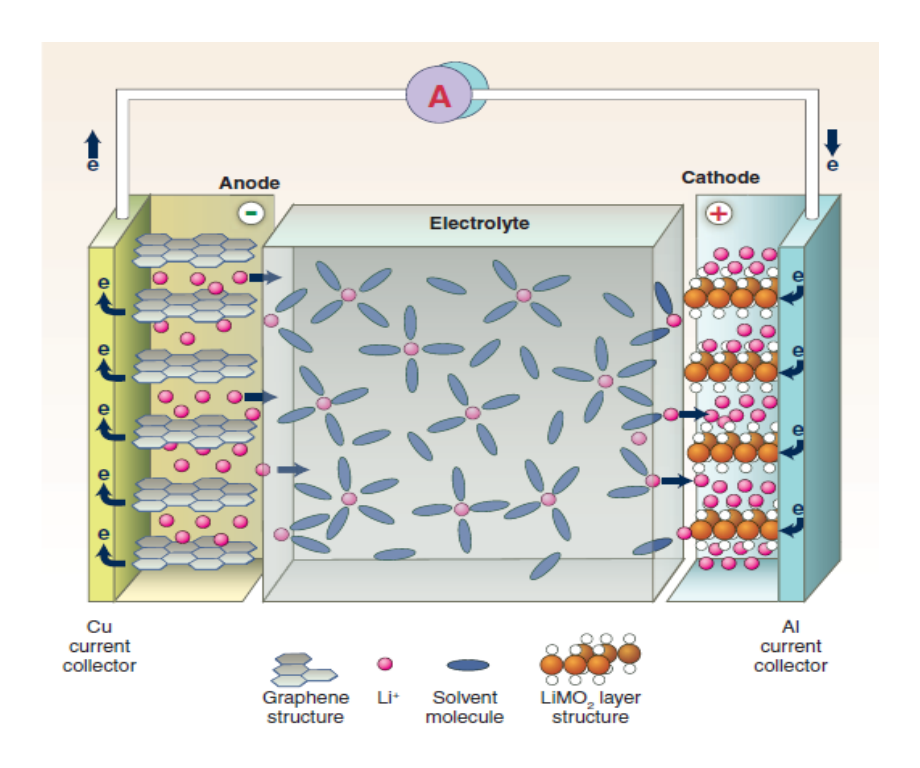


Figure 3. Schematic of a lithium ion battery (LIB) (Dunn et al. 2011)

The production cost, over-temperature sensitivity, and internal pressure buildup are related to minimizing the hazards associated with liquid electrolytes inside LIBs. Thus, the development of alternative electrolytes that can enable beyond Li-ion advanced battery technologies are necessary to keep up with the demands for vehicle electrification. (Bruce et al. 2011) Optimizing beyond Li-ion battery systems will provide EVs with the specific energy required for longer travel distances between recharging. (Bruce et al. 2011) The following section will discuss how solid-state electrolytes can enable solid-state batteries for electrical vehicles.

#### 1.3 Need for solid state electrolytes

State-of-the-art lithium-ion batteries, with a specific energy of ~150 Wh kg<sup>-1</sup> do not yet have sufficient energy or life for use in electrified vehicles that would match the performance of internal combustion vehicles. Energy densities two and five times greater are required to meet the

performance goals of a future generation of plug-in hybrid-electric vehicles (PHEVs) with a 40-80 mile all-electric range, and all-electric vehicles (EVs) with a 300 to 400 mile range, respectively. Further improvements in energy density of factors of two to three may yet be achievable for SOA Li-ion systems; factors of five or more may be possible for lithium-oxygen systems (Thackeray et al. 2012).

The specific energy necessary to obtain a 300 to 400 mile range EV is between 350 and 400 Wh kg<sup>-1</sup> (Song et al. 2013). The battery chemistries that can enable a specific energy greater than this would be a Li-S or a Li-air (Bruce et al. 2011). A Li-S system possesses a theoretical specific energy of ~1168 Wh kg<sup>-1</sup>, and a Li-air system of ~1752 – 2691 Wh kg<sup>-1</sup> (Thackeray et al. 2012). Neither are yet commercialized, however, due to several technical challenges. For both chemistries, metallic lithium would be used as the anode. The overwhelming appeal of Lielectrochemistry lies in its low molecular weight; small ionic radius, which is beneficial for diffusion; and low redox potential (Eo(Li+/Li)=-3.04V vs. standard hydrogen electrode (SHE)). The latter enables high-output voltages and therefore high-energy densities. (Etacheri, 2011 and Dunn, 2011)

The nature of the highly active lithium battery chemistry places severe electrochemical requirements on the electrolyte. The organic electrolytes invariable rely on the formation of a protective Solid Electrolyte Interphase (SEI) layer to limit the reaction or decomposition rate. Conductive electron paths may be formed along lithium dendrites for liquid or polymer electrolytes, while grain boundaries, pores, or cracks may become electronic paths for glass and ceramic electrolytes (Nazri et al. 2003). Therefore, an electrochemically and chemically stable solid electrolyte is required.

#### 1.4 Inorganic solid state Li-ion conductors

When cycling a lithium battery, several electrochemical reactions may take place at the electrodes as a function of the voltage range. The decomposition of organic electrolytes at the negative electrode has been a major concern, as there is no organic electrolyte that can tolerate the reducing power of metallic lithium or lithium doped graphite (commonly used in Li-ion batteries). (Nazri et al. 2003) In fact, the reason that current anodes work so well is mainly because of the formation of a protective layer on the surface of the anode. This protective layer is formed by decomposition of organic solvents (SEI layer). The nature of SEI depends on the organic solvents used in the battery. The SEI is electronically insulating, but has significant lithium ion conductivity and serves as a protective layer to prevent further reaction between the liquid electrolyte and graphite. (Nazri et al. 2003)

The average voltage of a Li-ion battery (LiC<sub>6</sub>//LiCoO<sub>2</sub>) is 3.75 V and its operating voltage range is between 3 to 4.5 V (Nazri et al. 2003). It has been found that different carbonate-based electrolyte solvents show stability above 5 V, providing the opportunity to use high voltage cathode materials (layered LiCoO<sub>2</sub> and 3-D spinel LiMn<sub>2</sub>O<sub>4</sub> cathodes) (Nazri et al. 2003). However, SOA Li-ion batteries use liquid electrolytes with low flash point solvents, and may present safety concerns, leakage and corrosion (Knauth, 2009).

If the organic solvent in the lithium battery can be replaced by inorganic Li-conducting solid materials, the following advantages are expected: no leakage of the electrolyte, broader operating temperature range (since inorganic solid electrolytes do not freeze, boil, or ignite), and only one type of carrier ion (Li-ion) migrates. Additionally, long life-time is expected because of little self-discharge (Adachi et al. 1996).

#### 1.4.1 Crystalline ceramic electrolytes

Among the inorganic solid state ion conductors, the Superionic conducting oxide (SCO) electrolytes show diverse features that make them attractive for solid-state batteries: typically synthesized in air and are reasonably stable in ambient air, high hardness, increasing conductivity with increasing temperature, along with the benefits associated of being a solid material. Hence, a review of the best understood and more promising ceramic electrolytes will be presented below.

#### 1.4.1.1 Perovskite

The perovskite structure, with the general formula ABO<sub>3</sub>, has can accommodate myriad ions, both aliovalent and isovalent, on both on the A and B lattice sites. This results in the introduction of vacancies in the lithium lattice (Huggins, 2009). The perovskite type Li<sub>3x</sub>La<sub>2/3-x</sub>TiO<sub>3</sub> (LLTO) shows excellent bulk Li-ion conductivity (>10<sup>-3</sup> S/cm) when x~0.3 (Inaguma, et al. 1994). Nevertheless, high temperature sintering is required for sample preparation and high Li<sub>2</sub>O losses are observed leading to difficulty in controlling Li-ion content and consequently, ion conductivity (Ban and Choi, 2001). Furthermore, instability at low potentials limits the utility of LLTO owing to its reduction at potentials below the Ti<sup>3+</sup>/<sup>4+</sup> redox reaction (1.5 V vs Li/Li<sup>+</sup>) (Klinger et al. 1997).

#### 1.4.1.2 NASICON-Type

The NASICON (Na SuperIonic conductor) crystallographic structure NaA2<sup>IV</sup>(PO4)3 (A<sup>IV</sup> = Ge, Ti and Zr) was identified in 1968 (Hagman and Kierkegaard, 1968). Among the Al-doped ceramics, the nominal composition Li<sub>1.3</sub>Al<sub>0.3</sub>Ti<sub>1.7</sub>(PO4)3 (LATP) was reported to have the optimum Li ionic bulk conductivity of 3 x  $10^{-3}$  S/cm at 298K. The substitution of Ti<sup>4+</sup> by smaller Al<sup>3+</sup> cations reduces unit cell dimensions of the NASICON framework and enhances ionic conductivity by about three

orders of magnitude. However, as for LLTO, these NASICON-Type materials are unstable with Li metal due to facile Ti<sup>4+</sup> reduction (Aono et al. 1990).

#### 1.4.1.3 LISICON and thio-LISICON Type

LISICON or <u>Li</u> <u>SuperIonic conductor structure</u> was named by Hong, H. Y-P (1978). The LISICON framework is related to the γ-Li<sub>3</sub>PO<sub>4</sub> crystal structure. Even in doped compounds the ionic conductivity is relatively low (about 10<sup>-6</sup> S/cm at room temperature). Furthermore, LISICON Li<sub>14</sub>ZnGe<sub>4</sub>O<sub>16</sub> is highly reactive with lithium metal and CO<sub>2</sub>. The thio-LISICON family possesses a higher Li ion conductivity than LISICON by the replacement of oxide ions by larger and more polarizable sulfide in the framework improving ionic mobility. Thio-LISICON compounds based on Li silicon sulfides have an even higher ionic conductivity of 6.4 x 10<sup>-4</sup> S/cm at room temperature for Li<sub>3.4</sub>Si<sub>0.4</sub>P<sub>0.6</sub>S<sub>4</sub>. (Kanno and Murayama, 2001).

#### 1.4.1.4 Garnet

Hyooma first proposed Li-ion conducting oxides with the garnet crystal structure (Hyooma and Hayashi, 1988). Garnets offer flexibility in multiple primary and sublattice cation sites. Weppner et al. (2007) discovered a high ionic conductivity formulation: Li<sub>7</sub>La<sub>3</sub>Zr<sub>2</sub>O<sub>12</sub> (LLZO). This material crystallizes in the tetragonal crystal structure without being doped. The addition of approximately 0.24 mole of Al<sup>3+</sup> is necessary to stabilize the preferred cubic crystal structure that exhibits isotropic lattice conductivities in the 0.4 mS/cm range at room temperature. It was shown that the cubic-tetragonal phase transition is also affected by the Li concentration (Thompson et al. 2014). Additionally, the grain boundary resistance is relatively low resulting in total conductivities that are comparable to the lattice conductivity and also exhibit an electrochemical window from 0 to 9 V vs. Li/Li<sup>+</sup>. (Ohta, 2011) Unlike LATP and LLTO, LLZO exhibits the combination of high total

ionic conductivity and stability against Li. The latter is achieved by using skeleton framework of cations (La, Zr, Ta, Al) that are not believed to be redox active at low potentials vs Li<sup>+</sup>/Li. (Sakamoto, 2014) However, Li-LLZO interfacial impedance is in the hundreds of ohms/cm range at room temperature, which is relatively high (Ohta, 2011). Additionally, a high processing temperature is required to bond or sinter components together which complicates cell fabrication (Sakamoto, 2014).

#### 1.4.2 Inorganic non-crystalline solid electrolytes

#### 1.4.2.1 LIPON

The thin-film lithium phosphorous oxynitride electrolyte (Lipon, Li<sub>2.9</sub>PO<sub>3.3</sub>N<sub>0.46</sub>), synthesized by sputtering Li<sub>3</sub>PO<sub>4</sub> in pure nitrogen, was found to have a conductivity of 2 x 10<sup>-6</sup> S/cm at room temperature and excellent long-term stability in contact with lithium. One of the Li/Lipon/TiS<sub>2</sub> cells, which had an open circuit voltage of about 2.5 V at full charge, underwent over 4,000 charge/discharge cycles (Bates et al. 1993). However, oxide-based glassy electrolytes such as Lipon have to be utilized as thin films to compensate for their low ionic conductivities, and their limited cell capacity is one of the disadvantages of thin-film batteries. Therefore, the development of highly conductive solid electrolytes is imperative to create large-sized, all-solid-state batteries with high capacity. (Mizuno and Hayashi, 2005)

#### 1.4.2.2 Sulfide glasses

The high conductivities and low activation energies of sulfide glasses compared to the oxide glasses is attributed to the weaker bonding of Li with the non-bridging sulfur anions, due to the higher polarizability and softer basicity of the sulfide ion (Nazri et al. 2009).

#### 1.4.2.3 Li<sub>2</sub>S-P<sub>2</sub>S<sub>5</sub>

Glassy solid electrolytes in the system  $\text{Li}_2\text{S}-\text{P}_2\text{S}_5$  are selected as typical sulfide solid electrolytes and have shown high lithium ion conductivities of  $10^{-4}$  to  $10^{-3}$  S/cm at room temperature (Mizuno et al. 2006). However, most of them show low chemical stability to moisture, as they tend to hydrolyze and generate  $\text{H}_2\text{S}$  gas (Ohtomo et al. 2013).

Glassy Li<sub>2</sub>S-P<sub>2</sub>S<sub>5</sub> (LPS) solid electrolytes are composed of lithium (Li<sup>+</sup>) and *ortho*-thiophosphate ions (PS<sub>4</sub><sup>3-</sup>) and its ionic conductivity is enhanced as the Li<sub>2</sub>S content is increased as the lithium source. The 70Li<sub>2</sub>S-30P<sub>2</sub>S<sub>5</sub> (mol%) glass-ceramic exhibits the highest conductivity of 3.2 x 10<sup>-3</sup> S/cm at room temperature and the lowest activation energy of 12 kJ/mol for conduction (Mizuno et al. 2006). Nevertheless, this composition is not the most chemically stable against air. Muramatsu et al. (2011) showed that the composition of 75Li<sub>2</sub>S-25P<sub>2</sub>S<sub>5</sub> (glass and glass-ceramic) generated the least amount of H<sub>2</sub>S (Figure 4) after exposure to air for one minute without a significant change after longer storage. Additionally, the sulfide electrolyte at this composition undergoes little structural change in air, which was confirmed by Raman spectroscopy before and after one day of exposure to the atmosphere (Muramatsu et al. 2011). 75Li<sub>2</sub>S-25P<sub>2</sub>S<sub>5</sub> possesses an adequate ionic conductivity, on the 10<sup>-4</sup> to 10<sup>-3</sup> S/cm range (Mizuno et al. 2006). Thus, 75Li<sub>2</sub>S-25P<sub>2</sub>S<sub>5</sub> glass and glass-ceramic are promising solid electrolytes for all-solid-state lithium batteries in terms of chemical stability and conductivity. (Muramatsu et al. 2011)

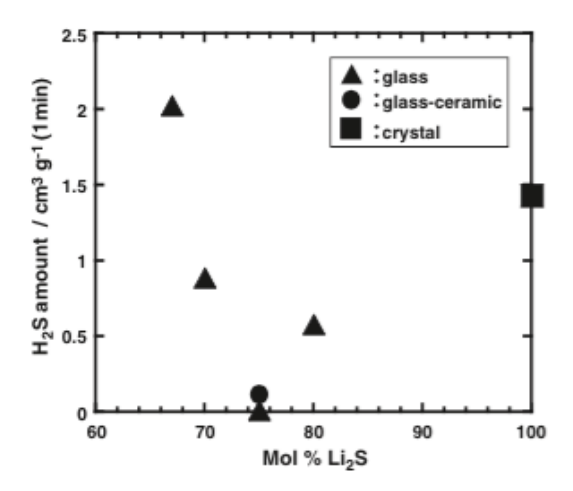


Figure 4. Amount of H<sub>2</sub>S generated from pelletized Li<sub>2</sub>S-P<sub>2</sub>S<sub>5</sub> (LPS) glasses with different Li<sub>2</sub>S contents (Muramatsu et al. 2011)

Highly conductive crystalline thio-LISICON analogues are formed by the crystallization of the mechanically milled Li<sub>2</sub>S-P<sub>2</sub>S<sub>5</sub> glasses. The names were coined due to the similarity between crystal structures. However, the glass-ceramics obtained by heating the Li<sub>2</sub>S-P<sub>2</sub>S<sub>5</sub> glasses have no germanium as the thio-LISICONs. The XRD patterns in regions I and III for the thio-LISICONS were indexed by a monoclinic superlattice cell of a x 3b x 2c, while the patterns in region II were indexed by that of a x 3b x 3c (Mizuno et al. 2006). A presumable explanation for the similarities on XRD patterns between the thio-LISICONs and the glass-ceramics is to assume that the Li-richer Li<sub>3+5y</sub>P<sub>1-y</sub>S<sub>4</sub> phases with a lack of phosphorus are formed in the glass ceramics. Murayama et al. (2004) found that the Li<sub>3+5y</sub>P<sub>1-y</sub>S<sub>4</sub> crystals in the Li<sub>2</sub>S-P<sub>2</sub>S<sub>5</sub> system were formed in the composition range of  $0 < y \le 0.27$ . Thus, the crystal structures of Li<sub>3.25</sub>P<sub>0.95</sub>S<sub>4</sub> and Li<sub>3.2</sub>P<sub>0.96</sub>S<sub>4</sub> would be similar to those of thio-LISICON II (Li<sub>3.25</sub>Ge<sub>0.25</sub>P<sub>0.75</sub>S<sub>4</sub>) and thio-LISICON III (Li<sub>3.2</sub>Ge<sub>0.2</sub>P<sub>0.8</sub>S<sub>4</sub>), respectively. (Hayashi et al. 2003).

In the case of the  $75\text{Li}_2\text{S}-25\text{P}_2\text{S}_5$  glass, the thio-LISICON III analogue is formed as the first precipitated crystal and remains up to 300°C. The crystals of Li<sub>3</sub>PS<sub>4</sub> and Li<sub>4</sub>P<sub>2</sub>S<sub>6</sub> are finally present at 550 °C (Hayashi et al. 2003).

Hayashi et al. (2003) found that the thio-LISICON II analogue with higher lithium content than the thio-LISICON III analogue was not formed in the 75Li<sub>2</sub>S-25P<sub>2</sub>S<sub>5</sub> glass but formed in the Liricher 80Li<sub>2</sub>S-20P<sub>2</sub>S<sub>5</sub> glass. The thio-LISICON II and III analogues have not been reported as thermodynamically stable crystals in the Li<sub>2</sub>S-P<sub>2</sub>S<sub>5</sub> system, which agreed with Hayashi et al. (2003) results in which these phases were not obtained by solid-phase reaction. Hence, these phases probably precipitated as a metastable phase from the mechanically milled Li<sub>2</sub>S-P<sub>2</sub>S<sub>5</sub> glasses, and they are changed to a stable crystal such as Li<sub>3</sub>PS<sub>4</sub> with an increase in temperature (Hayashi et al. 2003). Crystals such as Li<sub>3</sub>PS<sub>4</sub> and Li<sub>4</sub>P<sub>2</sub>S<sub>6</sub> has been reported to show a low conductivity below of  $10^{-7}$  S cm<sup>-1</sup> at room temperature (Tachez et al. 1984).

The emphasis of this work is to develop a better understanding of the effect of hot pressing temperature on the microstructure and electrochemical performance of 75Li<sub>2</sub>S-25P<sub>2</sub>S<sub>5</sub> as a potential solid electrolyte for electric vehicle batteries.

The following section will focus on the techniques conducted to prepare and characterize the microstructure and electrochemical stability of the 75Li<sub>2</sub>S-25P<sub>2</sub>S<sub>5</sub> samples.

#### 1.5 Ceramic electrolyte processing and characterization techniques

#### 1.5.1 Planetary ball milling

The mechanical milling technique, which uses a high-energy ball mill, has attracted much attention as a new procedure for preparing inorganic amorphous/metastable materials instead of a

conventional melt-quenching method. (Hayashi et al. 2001) It was first demonstrated for Li<sub>2</sub>S-SiS<sub>2</sub> compositions and then expanded to the Li<sub>2</sub>S-P<sub>2</sub>S<sub>5</sub>. (Nazri et al. 2003) The use of mechanochemical milling offers several advantages over the melt quenching method: i) basically a room temperature process, and 2) total energy consumed is still less than that used in a melt-quench process even though achieving complete amorphization requires about 20 hours of milling time. Additionally, the resulting fine-grained powder is ready to fabricate directly as a pressed pellet or as the electrolyte layer in a compacted solid-state battery. In comparison, the lithium ion conductivities achieved by ball milling were as high or nearly as high as that of glasses prepared by rapid quench of the same composition. (Hayashi et al. 2001; Nazri et al. 2003)

Hayashi et al. (2002) obtained sulfide glassy electrolytes that exhibited high Li-ion conductivities over 10<sup>-4</sup> S/cm at room temperature, a wide electrochemical potential window of 10V, and also reported that the crystallization of the Li<sub>2</sub>S-P<sub>2</sub>S<sub>5</sub> glasses prepared by mechanical milling improves their conductivities.

For this work, Li<sub>2</sub>S-P<sub>2</sub>S<sub>5</sub> amorphous material was prepared from Li<sub>2</sub>S and P<sub>2</sub>S<sub>5</sub> (reagent-grade Aldrich, 99%) crystalline powders. The mixture was mechanically milled at room temperature by a planetary ball-mill apparatus (Fritsch Pulverisette 7) using an alumina jar (volume of 45 mL) with twenty alumina balls, 10 balls of 10 mm in diameter and ten balls of 5 mm in diameter. The milling time was 20 h and the rotation speed was 370 rpm. All the processes were performed in a dry, Ar-filled glove box. In this work, Dr. Mizuno from Toyota (Ann Arbor, MI), prepared LPS powders for hot pressing and DC cycling experiments at MSU.

#### **1.5.2** Densification of sulfide electrolytes

The temperature at which the sulfide experiences the transition from a rigid glass to a rubbery state is termed the glass transition temperature ( $T_g$ ).  $T_g$  is a function of the heating/cooling rate; the transition temperature shifts to higher temperatures with increasing heating rates. The viscosity of a glass at  $T_g$  is quite large and on the order of  $10^{15}$  Pa\*s, which in turn implies that atomic mobility is quite low (Barsoum 2003). The transition temperature can be determined by measuring the specific volume as a function of the heating/cooling rate (Figure 5). The temperature at which the property changes slope continuously is defined as the glass transition temperature (Barsoum 2003).

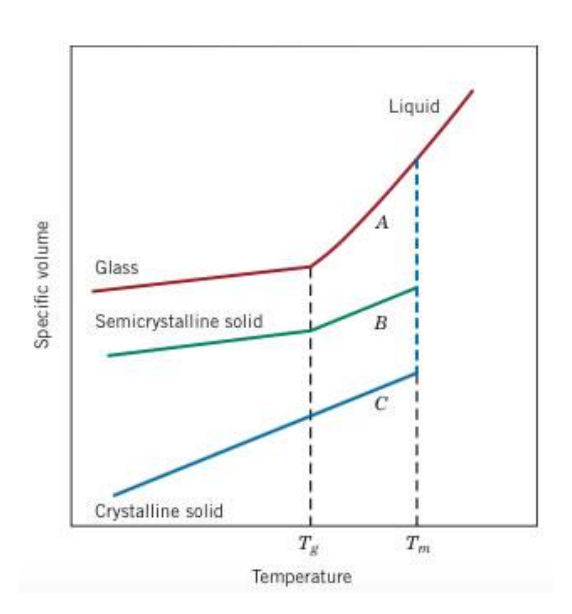


Figure 5. Schematic of specific volume changes observed as a glass is heated through Tg (Callister 2007)

The sulfide glass crystallizes between  $T_{\rm g}$  and the melting point. For the crystalline material, there is a discontinuous change in specific volume at the melting temperature  $T_{\rm m}$ . The profile for the totally amorphous material is continuous bus experiences a decrease in slope at the glass transition temperature. The behavior is intermediate between these extremes for a semicrystalline material in

that both melting and glass transition phenomena are observed;  $T_m$  and  $T_g$  are properties of the respective crystalline and amorphous phases in this semicrystalline material. The behaviors represented in this figure will depend on the rate of cooling or heating (Callister 2007)

A material microstructure can be altered by heating it to a temperature T below its melting temperature through sintering. Typically 2/3 T<sub>m</sub> < T < T<sub>m</sub>. The macroscopic driving force operative during sintering is the reduction of the excess energy associated with surfaces. This can happen by 1) reduction of the total surface area by an increase in the average size of the particles, which leads to coarsening, and/or 2) the elimination of solid/vapor interfaces and the creation of grain boundary area, followed by grain growth, which leads to densification. These two mechanisms are usually in competition. If densification dominates, the pores get smaller and disappear with time and the compact shrinks, but if the atomic processes that lead to coarsening are faster, both the pores and grains get larger with time (Barsoum 2003).

Dense pellets of sulfide electrolytes can be obtained by pressing at room temperature. In the case of Li<sub>2</sub>S-P<sub>2</sub>S<sub>5</sub> glasses, densification results from cold pressing. The relative density increases with increasing applied pressure:

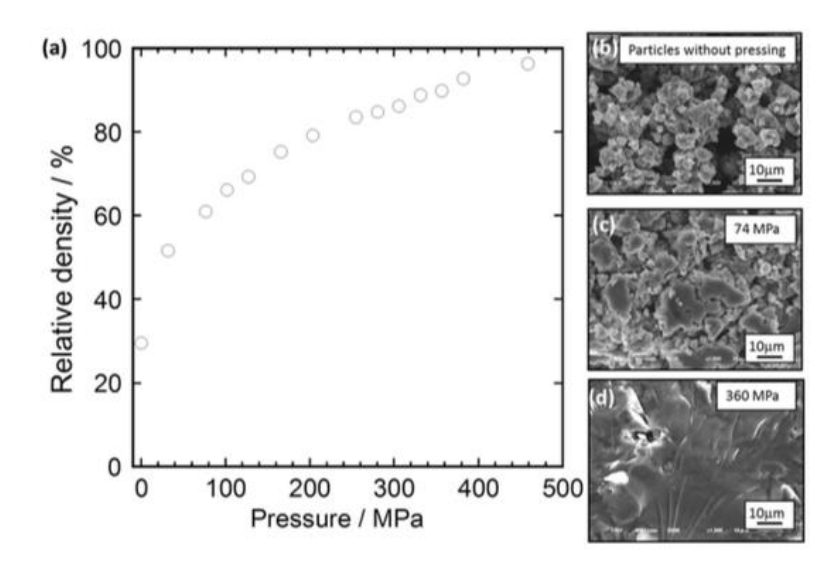


Figure 6. a) Densification pressure dependence of 75Li<sub>2</sub>S-25P<sub>2</sub>S<sub>5</sub> (mol%) glass solid electrolyte, b) SEM image of 75Li<sub>2</sub>S-25P<sub>2</sub>S<sub>5</sub> glass powder. SEM images of fracture cross-sections of 75Li<sub>2</sub>S-25P<sub>2</sub>S<sub>5</sub> glass powders pressed at c) 74 and d) 360MPa (Sakuda et al. 2013)

The relative density exceeds 90% when the 75Li<sub>2</sub>S-25P<sub>2</sub>S<sub>5</sub> glass powder is compressed by a pressure of over 350MPa. Thus, 75Li<sub>2</sub>S-25P<sub>2</sub>S<sub>5</sub> glass with a remarkably high relative density can be obtained by pressing without heat treatment as it was confirmed by Scanning Electron Microscopy images (Figure 5.b-d) by the quantity of pores observed per unit area/volume. This behavior is seen in the Li<sub>2</sub>S-P<sub>2</sub>S<sub>5</sub> system due to the relatively low Young's modulus making room temperature densification effective (Sakuda et al. 2013). By hot-pressing the solid electrolyte near the glass transition temperature (~170 °C), higher density pellets were attained (Kitaura 2011).

Kitaura et al. (2011) optimized the hot pressing temperature and time of 80Li<sub>2</sub>S-20P<sub>2</sub>S<sub>5</sub> powders to obtain an entirely translucent pellet. The degree of densification was evaluated qualitatively:

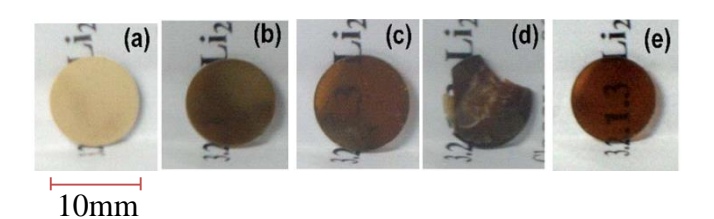


Figure 7. Photographs of the pellets of the 80Li<sub>2</sub>S-20P<sub>2</sub>S<sub>5</sub> sample pressed at a) room temperature, b) 180°C, c) 210°C and d) 240°C for 2h, and e) 210°C for 4h (Kitaura et al. 2011)

From the pictures shown above, the translucent pellet was obtained by pressing at 210°C for 4h under 360MPa. The translucence of the pellet pressed at 200°C was ascribed to an increase in transmittance by the disappearance of voids between particles or an increase in density. The transition from amorphous to glass occurred by pressing around the glass transition temperature. In contrast, crystallization and light scattering off grain boundaries leads to an opaque pellet (d) after pressing around the crystallization temperature of 240°C. Moreover, the pellet pressed at 210°C showed the higher conductivity of 8.8 x 10<sup>-4</sup> S/cm compared to the conductivity of 3.7 x 10<sup>-4</sup> S/cm in the pellet pressed at room temperature. The decrease in grain boundary and voids increased the conductivity of the different samples (Kitaura et al. 2011).

Measuring a solid electrolyte shear modulus is important to predict lithium dendrite penetration across a solid electrolyte (Monroe and Newman 2005). According to Newman et al, dendrite propagation is prevented when the shear modulus is three or more orders of magnitude higher than that of metallic Li ( $\geq$ 20 GPa). The latter also implies a high relative density and almost negligible interconnected porosity. Sakuda et al. (2013) measured the Young modulus of Li<sub>2</sub>S-P<sub>2</sub>S<sub>5</sub> glassy solid electrolytes for four different Li<sub>2</sub>S contents (figure 7) High-density pellets were prepared by hot pressing at their respective glass transition temperatures. The Young's modulus of xLi<sub>2</sub>S\*(100-x)P<sub>2</sub>S<sub>5</sub> (mol%) glasses (x = 50 - 80) increased with increasing Li<sub>2</sub>S content. The

Young moduli are in the range of 18-25 GPa.  $75\text{Li}_2\text{S}*25\text{P}_2\text{S}_5$  showed a Young's modulus of 24 GPa. (Sakuda et al. 2013)

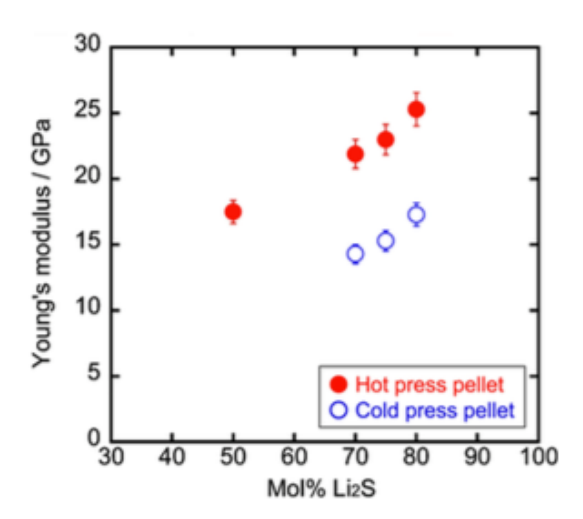


Figure 8. Young's modulus of  $xLi_2S*(100-x)P_2S_5$  (mol%) glass pellets prepared by hot press and cold press at 360 MPa (Sakuda et al. 2013)

In the present work, the amount of sample (~0.5g), time at target temperature (4h), cold-press (360MPa) and hot-press pressure (47MPa) were held constant while the target temperature was varied from 130 to 190°C with increments of 10°C between temperatures. The sample was compressed in a half-inch stainless steel (SS) die with two SS half-inch plungers in a double acting configuration and heated up by resistance heating.

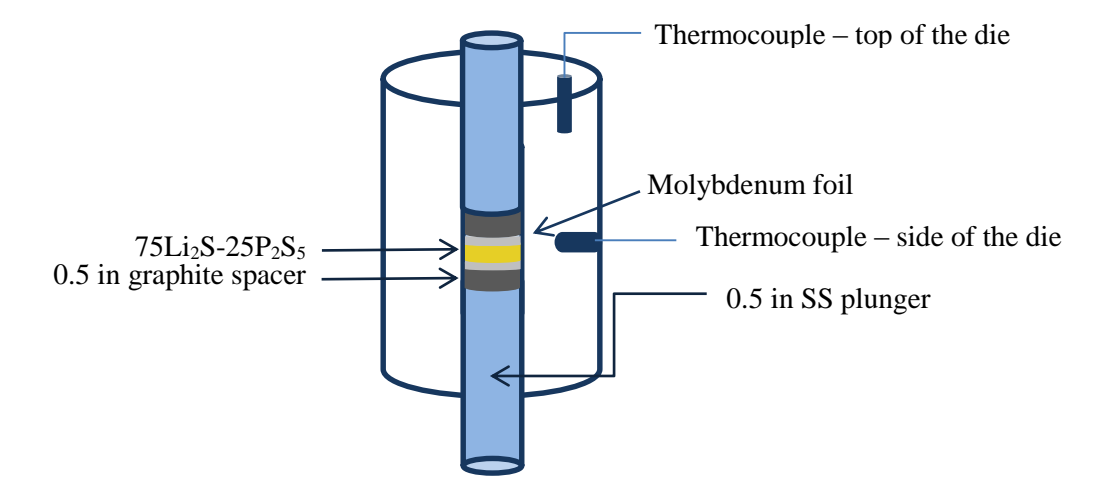


Figure 9. Schematic of a double acting die configuration

#### 1.5.3 Electrochemical characterization

#### 1.5.3.1 Electrochemical Impedance Spectroscopy (EIS)

EIS is a technique for characterizing the conductivity of electrolytes. AC (alternating current) impedance measurements are made over a range of frequencies to separate transport phenomena based on their relaxation times or time constants (Irvine et al. 1990). In a typical EIS experiment (Figure 9), the solid electrolyte is located between two ionically-blocking interfaces (also known as blocking electrodes) that are adjacent to the electronic conductors employed as electrodes. Generally, it is assumed that the electrical current within the solid phase between the electrodes is carried by ionic species, but they are blocked at the electrolyte/electrode interface, whereas the transport of electrons is not. The experimental results, impedance data, are represented in the form of imaginary (capacitive) against real (resistive) impedances. (Huggins, 2009; Irvine et al. 1990)

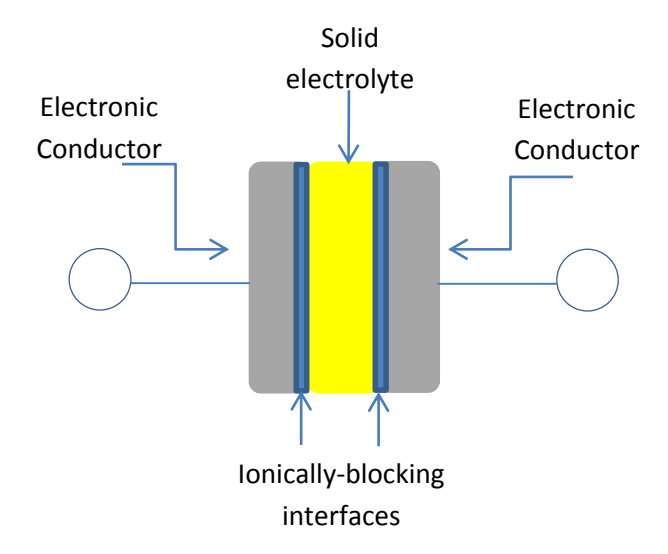


Figure 10. Experimental arrangement generally used for variable frequency AC measurements to evaluate ionic transport in a solid electrolyte

An equivalent circuit can model the frequency dependent data described. The interface of a solid electrolyte, considered a purely ionic conductor, and a purely electronic conductor can be represented as a parallel plate capacitor. The electrolyte acts as a resistance that the charge must pass and the capacitive properties of the two electrolyte/electrode interfaces are combined into a single capacitance ( $C_{int}$ ). An electrical equivalent circuit that consists of the resistance arranged in series with the capacitance represents the low-frequency behavior of an electrochemical cell.

At higher frequencies, an additional capacitance that corresponds to the presence of the electrolyte with a finite dielectric constant must be included ( $C_{geom}$ ). This new configuration, or *Debye circuit*, in which the extra parallel capacitance acts across the whole configuration, can be represented as following:

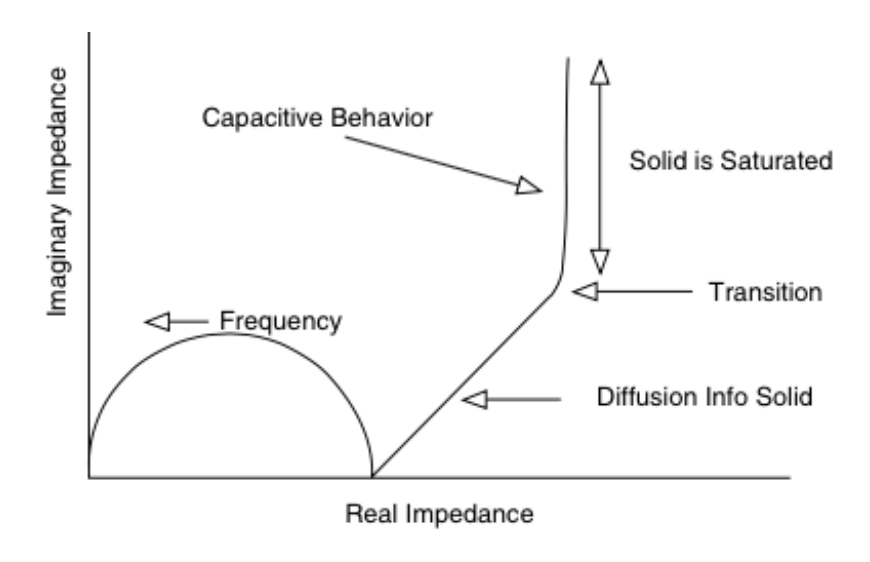


Figure 11. Schematic complex plane plot of the Debye equivalent circuit (Huggins, 2009)

Each parallel resistive-capacitive element gives rise to a semicircle from which the resistance and capacitance values may be extracted (Irvine et al. 1990). Through the evaluation of the relative values of the intercepts upon the real impedance axis provides information about the ionic or total resistance. Based on the frequency response of each transport phenomenon, a semi-circle arises over a range of capacitance values as shown in the table below

Capacitance (F)	Phenomenon Responsible
10 <sup>-12</sup>	Bulk
10 <sup>-11</sup>	Minor, second phase
$10^{-11} - 10^{-8}$	Grain boundary
$10^{-10} - 10^{-9}$	Bulk ferroelectric
10 <sup>-9</sup> - 10 <sup>-7</sup>	Surface layer
10 <sup>-7</sup> - 10 <sup>-5</sup>	Sample-electrode interface
10 <sup>-4</sup>	Electrochemical reactions

Table 1. Capacitance values and their possible interpretation (Irvine et al. 1990)

The interface between electrolyte and electrode can give information on the nature of the conducting species within the electrolyte by the impedance response measured. A common experimental observation is that the low-frequency tail in complex impedance plots is not truly vertical, as it would be expected for a completely blocking electrode interface that acts like a frequency-independent electrical double-layer capacitance. A straight line inclined at a finite angle from the vertical is observed when the electroactive species is not blocked at the interface, but diffuses into or out of one or both the electrodes due to solubility between the mobile ion and the electrode. According to Fick's second law, the low-frequency data are represented by a straight line with a slope of 45°. This involves the introduction of "admittance", or "Warburg impedance", into the equivalent circuit. (Huggins, 2009)

Surface layers are another type of phenomenon that can be analyzed through impedance spectroscopy, which are often found on ceramics or glasses. The presence of this "film" appears in the spectrum as a semicircle at lower frequencies. Without this layer the low-frequency behavior expected would be a nearly vertical line representing charge build-up at the blocking metal electrodes. It is then possible to study the conditions for formation/removal of the surface layer and the associated kinetics. (Irvine et al. 1990)

In the present study, Li-ion conductivity of 75Li<sub>2</sub>S-25P<sub>2</sub>S<sub>5</sub> and total cell resistance was determined using AC Electrochemical Impedance Spectroscopy (EIS) through Nyquist plots (Figures 17 – 20). A VersaSTAT4 potentiostat covered the frequency range of 50 mHz to 800 kHz, with an applied voltage of 20mV, nickel pins as current collectors and Li metal as non-blocking electrodes. The cells were tested after the sample powders were densified into pellets with 12.7 mm in diameter and ~ 2 mm in thickness (see table 2 and 3 for accurate measurements) in a custom

designed load frame that applied a constant pressure of 316 kPa during electrochemical measurements.

#### 1.5.3.2 Preconditioning

A DC technique used to pass Li-ions through the LPS pellets moving between Li metal anodes. A low current density of  $0.01 \text{mA/cm}^2$  was applied in both directions to acquire a stable interphase between the electrodes and electrolyte. Room temperature preconditioning of 10 cycles was conducted on the eight pellets that were tested through AC impedance measurements and DC asymmetric polarization tests. Seven hot-pressed pellets were pressed between  $130^{\circ}\text{C}$  and  $190^{\circ}\text{C}$ . To serve as a baseline, one pellet was pressed at room temperature.

#### 1.5.3.3 DC asymmetric polarization method

Attempting to demonstrate the maximum current density that LPS can withstand was above 1mA/cm² (relevant for EVs), a range of current densities was applied to the solid electrolyte. This test begins by applying a low current density of 0.01 mA/cm² for an hour in one orientation, follow by a 0 V hold to re-equilibrate the cell to open circuit equilibrium conditions. The DC polarization and 0V hold was followed by an AC impedance measurement to determine the impedance of the cell. After the AC measurement another 0 V hold for thirty minutes was used to re-equilibrate the cell. After the 0.01 mA/cm² hold, higher current densities were applied using the same sequence of 0V holds and EIS. The range of current densities was: 0.01, 0.05, 0.1, 0.5 and 1.0 mA/cm². If the Li/LPS/Li cell is stable, ohmic behavior is expected. If lithium metal penetrates, deviation from ohmic behavior should be observed and manifested as a drop in polarization voltage since Li metal propagating reduces cell resistance. Asymmetric, as opposed to symmetric, cycling

was used to allow the tracking of the trajectory of lithium metal propagating from one Li anode to the opposite anode.

#### 1.6 Materials characterization techniques

#### 1.6.1 X-Ray Diffraction (XRD)

X-Ray Diffraction is a technique used to identify crystalline phases present in materials and to measure the structural properties (strain state, grain size, phase composition, preferred orientation and defect structure) of these phases. The intensities measured as a function of diffraction angle can provide quantitative, accurate information about long range atomic order. It is more sensitive to high Z-elements, since X-ray diffraction occurs off the electron shell. Thus, the diffraction peak intensity is higher for large Z-elements than low Z-elements (Brundle et al. 1992)

For this work, the crystallinity as a function of hot pressing temperature was characterized by X-Ray diffraction measurements on a Rigaku Smartlab diffractometer using Cu K $\alpha$  1.54 radiation within the 2 $\theta$  range of 10-70°. Before the measurements, the samples were grinded into powder and then sealed with Kapton film in an argon-filled glove box to avoid any moisture contamination from the atmosphere. Measurements were obtained at Toyota Motor Engineering & Manufacturing North America, Inc, Ann Arbor, MI.

#### **1.6.2** Differential Scanning Calorimetry (DSC)

Many of the physical or chemical transformations are associated with heat absorption or exothermic processes. DSC measures the differential heat flow between an inert reference and the sample upon heating or cooling at a particular rate or under isothermal conditions. Only in the case of a thermal event characteristic of a particular material, the differential heat flow will exist. Unlike differential thermal analysis (DTA), DSC can quantify the thermal events. (Sibilia, 1988)

For this work, Differential Scanning Calorimetry was conducted in a TA instrument, Q-100 under nitrogen gas flow. The samples were loaded in a hermetic pan and then closed with the corresponding lid in an Argon-filled glove box to keep the inert environment. The weight of the sample was measured in advance and the generated heat was monitored as a function of temperature. The scan rate was changed in the range between 0.7 and 5°C/min. Measurements were obtained at Toyota Motor Engineering & Manufacturing North America, Inc, Ann Arbor, MI.

#### **1.6.3** Scanning Electron Microscopy (SEM)

SEM provides high depth of field, high magnification topographic analysis. The resolution of these instruments is approximately two orders of magnitude better than optical microscopes and one order of magnitude less than transmission electron microscopes (TEM), thereby bridging the gap between these related techniques. SEM imaging is often preferred in place of optical imaging because of the enhanced depth of field. (Sibilia, 1988)

For this work, the morphology of the samples was studied using a Field Emission JEOL JSM-7800F Scanning Electron Microscope. The samples were sealed in an air-free vessel under argon inside of a glove box and transferred to the SEM chamber without air contamination.

Measurements were obtained at Toyota Motor Engineering & Manufacturing North America, Inc, Ann Arbor, MI.

# 2. The effect of hot pressing temperature on the electrochemical stability of $\text{Li}_2\text{S-P}_2\text{S}_5$ (75 – 25 % mole)

#### 2.1.Introduction

LPS is an attractive solid electrolyte to enable solid-state batteries employing metallic Li anodes, owing to its high ionic conductivity (~1mS/cm) at 25 °C and low cost (Takamasa, 2013; Takeuchi, et al. 2014). Therefore, its stability against metallic lithium must be understood. The purpose of this work was to characterize the effect of LPS processing conditions and their effect on Li stability. Typically, LPS-based electrolytes are densified at room temperature through the application of several hundreds of MPa (Sakuda). While relative densities in the 90 % range may be acceptable to study ionic transport measurement using EIS, higher densities may be necessary to prevent Li metal penetration during DC cycling of batteries. It follows that, hot pressing LPS was investigated to increase relative density. Moreover, by hot pressing, we tried to gain a better understanding how the densification conditions may affect LPS microstructure, chemical stability and electrochemical performance.

A series of experiments was conducted to characterize the effect of the hot pressing temperature on the bulk and electrochemical properties of 75Li<sub>2</sub>S-25P<sub>2</sub>S<sub>5</sub>. Two groups of 7 pellets were hot-pressed from 130°C to 190°C plus two cold-pressed pellets were left as base-line for comparison to the hot-pressed pellets (Table 2 and 3). To characterize the effect of hot pressing temperature and DC cycling, the changes in the atomic ordering and microstructure were characterized using differential scanning calorimetry (DSC), X-ray diffraction (XRD), optical microscopy, and scanning electron microscopy (SEM). Further, the electrical (ionic and electronic) properties were characterized using AC impedance measurements.

#### 2.2. Results and Discussion

## 2.2.1. Evaluating the effect of hot pressing temperature on LPS bulk properties

Since hot-pressing is known to promote chemical bonding between particles (Barsoum 2003), it is expected that hot-pressed pellets should be less prone to Li dendrite penetration compared to cold-pressed LPS. Furthermore, hot-pressing can reduce the porosity of the sample and presumably increase the Shear Modulus of the material. Monroe et al (2005) showed that if a solid-electrolyte has a shear modulus of  $\geq 20$  GPa, Li dendrites should not propagate. The purpose of this work was to attain the highest density pellet by hot pressing LPS amorphous material near the glass transition temperature.

#### 2.2.1.1. Densification conditions

Kingery (1963) stated that to achieve the highest densities, the principal considerations are extremely small particle size starting material and the temperature at which the powder transforms to a strong, dense body upon heating. Typically, 2/3 of the homologous temperature is the minimum hot-press temperature required to establish chemical bonding. However, in this work, hot-pressing was conducted below the LPS homologous temperature (~ 673 K) (Minami, K), to prevent crystallization, which occurs at approximately 220 °C based on DSC profiles (Figure 13). Additionally, Sakuda et al. 2013 showed that hot-pressing was effective in densifying comparable LPS formulations below 2/3 the homologous temperature.

The temperature regime selected covered the glass transition temperature (T<sub>g</sub>) region obtained from a DSC analysis with a heating rate of 5°C/min, identified between 140°C and 180°C. Nevertheless, a broader temperature range was used with the supposition that the crystallization

temperature along with the glass transition temperature may change with an applied pressure to the system. The temperature range selected was between 130°C and 190°C.

The hot pressed samples had a relative density between 72±1% and 86±1%, being the lowest at 180°C and the highest at 140°C (Table 2 and 3). The relative densities obtained for the samples pressed at room temperature were 77±1% and 80±1%. No clear correlation between hot pressing temperature and relative density can be concluded from this data set even though previous work from Sakuda et al. (2013) and Kitaura et al. (2011) showed that translucent pellets can be attained at pressures above 350MPa during four hours of hot-pressing time. Although it may be taken into account that for this work, crack-free pellets could not be obtained by cold-pressing and hot-pressing at 360MPa due to residual stress presumably. Therefore, cold-press pressure and hot-press pressure were fixed at 360MPa and 47MPa, respectively (Figure 11). 47 MPa was selected as the hot pressure because previous experiments (not shown) demonstrated this pressure can produce crack-free, hot-pressed LPS pellets. After hot-pressing, the relative density was determined using a theoretical 1.88 g cm<sup>-3</sup> corresponding to a 75Li<sub>2</sub>S-25P<sub>2</sub>S<sub>5</sub> transparent pellet obtained by Sakuda, et al. (2013), hot-pressed at 190°C at 360 MPa. Following are the samples prepared for this study. The pressing conditions and pellet properties are listed in Table 2.

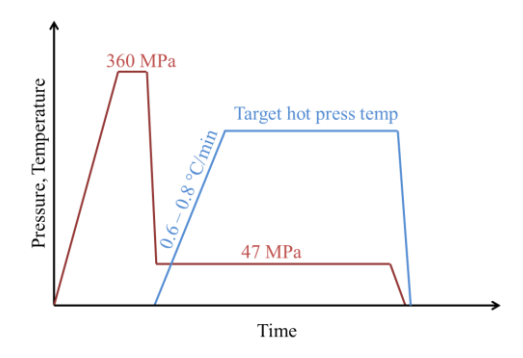


Figure 12. Schematic of the pressure and temperature profiles followed during hot pressing tests

Temperature	Room temperature- CP - B	130°C (HP-21)	140°C (HP-22)	150°C (HP-23)	160°C (HP-24)	170°C (HP-25)	180°C (HP-26)	190°C (HP-27)
Appearance		6	6		6	1		
Batch	59	44	45	46	47	48	49	50
Thickness (mm)	2.02	2.30	2.40	1.90	2.29	2.36	2.08	2.26
Average temperature, top of the die (°C)	N/A	112.1±1.9	130.0±0.7	104.0±0.6	148.4±1.0	161.4±1.4	178.8±4.4	178.1±5.3
Average temperature, side of the die (°C)	N/A	130.4±0.6	140.4±0.9	150.2±0.8	160.4±0.8	170.4±2.2	180.5±0.9	190.1±1.3
ΔT (°C)	N/A	18.3±2.0	10.4±1.2	46.1±1.0	12.0±1.3	9.0±2.6	1.7±4.5	12.0±5.4
Time at target temperature (h)	N/A	4.0	4.0	4.0	4.0	4.0	4.0	4.0
Cold-pressed pressure (MPa)	360	360	360	360	360	360	360	360
Hot-pressed pressure (MPa)	N/A	47	47	47	47	47	47	47
Average trace of oxygen (ppm)	1.10	0.67	0.80	1.15	1.23	0.94	0.71	1.05
Density, g/cm <sup>3</sup> (relative density, %)	1.50 (80)	1.51 (80)	1.62 (86)	1.51 (80)	1.53 (81)	1.46 (78)	1.54 (82)	1.45 (77)

Table 2. 75Li<sub>2</sub>S-25P<sub>2</sub>S<sub>5</sub> hot pressed pellets (12.7mm in diameter) between 130°C and 190°C for electrochemical performance analysis—Data set no.1

Temperature	Room temperature CP - A	130°C (HP-28)	140°C (HP-29)	150°C (HP-30)	160°C (HP-31)	170°C (HP-32)	180°C (HP-33)	190°C (HP-34)
Appearance	4							
Batch	58	51	52	53	54	55	56	57
Thickness (mm)	2.22	2.28	2.32	2.42	2.28	2.29	2.22	2.08
Average temperature, top of the die (°C)	N/A	121.6±3.9	121.8±1.0	152.1±3.7	151.8±3.7	155.2±1.3	160.2±1.0	176.8±2.4
Average temperature, side of the die (°C)	N/A	130.0±1.2	140.7±1.2	150.2±1.3	160.8±0.5	170.3±1.6	180.4±0.9	190.6±0.9
ΔT (°C)	N/A	$8.5\pm4.1$	18.9±1.6	1.9±4.0	9.0±3.8	15.1±2.0	20.1±1.4	13.8±2.6
Time at target temperature (h)	N/A	4.0	4.0	4.0	4.0	4.0	4.0	4.0
Cold-pressed pressure (MPa)	360	360	360	360	360	360	360	360
Hot-pressed pressure (MPa)	N/A	47	47	47	47	47	47	47
Average trace of oxygen (ppm)	1.22	1.25	1.78	1.77	1.74	1.63	1.23	1.27
Density, g/cm <sup>3</sup> (relative density, %)	1.45 (77)	1.36 (72)	1.41 (75)	1.40 (75)	1.48 (79)	1.39 (74)	1.35 (72)	1.39 (74)

Table 3. 75Li<sub>2</sub>S-25P<sub>2</sub>S<sub>5</sub> hot pressed pellets (12.7mm in diameter) between 130°C and 190°C for materials characterization—Data set no.2

The SEM micrographs (Figure 12) confirmed there is no significant difference in the microstructure with increased hot-press temperature; qualitatively the porosity appears to be more or less the same between samples.

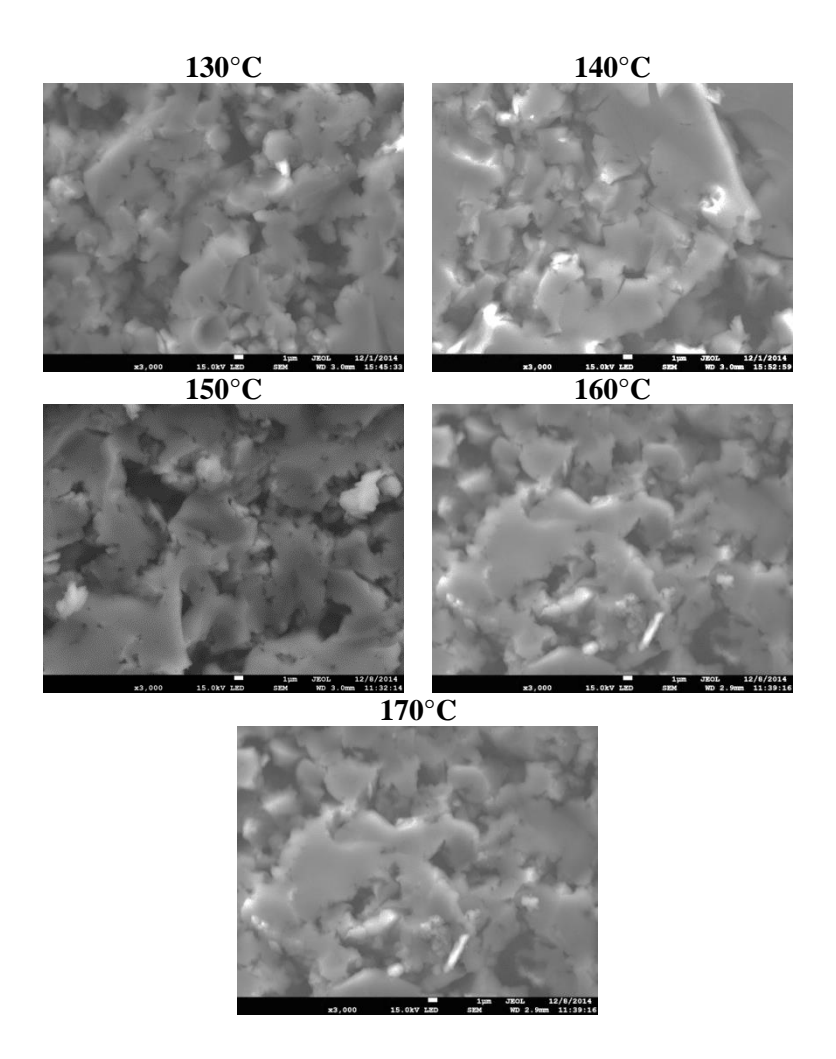


Figure 13. Fractured surfaces of hot-pressed samples between 130°C and 170°C

### **2.2.1.2.** Chemical transformations

Differential Scanning Calorimetry (DSC) was performed to detect a physical or chemical transformation on the bulk properties of LPS. DSC analysis revealed that all LPS powder prepared by planetary ball milling used in DC cycling tests is sufficiently comparable between batches, having a crystallization peak within the range of 220-230°C (Figure 13, heating rate of 5°C/min) except for batch 49 (hot pressed at 180°C) that showed an extra peak in the range of 190 – 200 °C. Therefore, the results obtained from this batch are not going to be considered in further discussions.

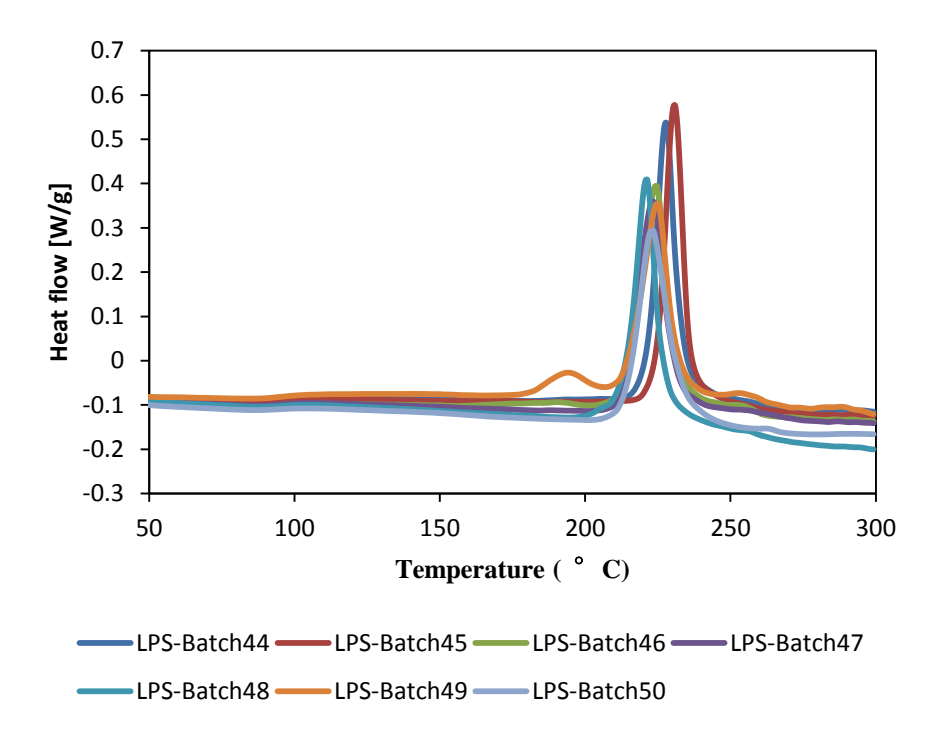


Figure 14. DSC spectra of Li<sub>2</sub>S-P<sub>2</sub>S<sub>5</sub> (75 – 25 % mole) powder as prepared

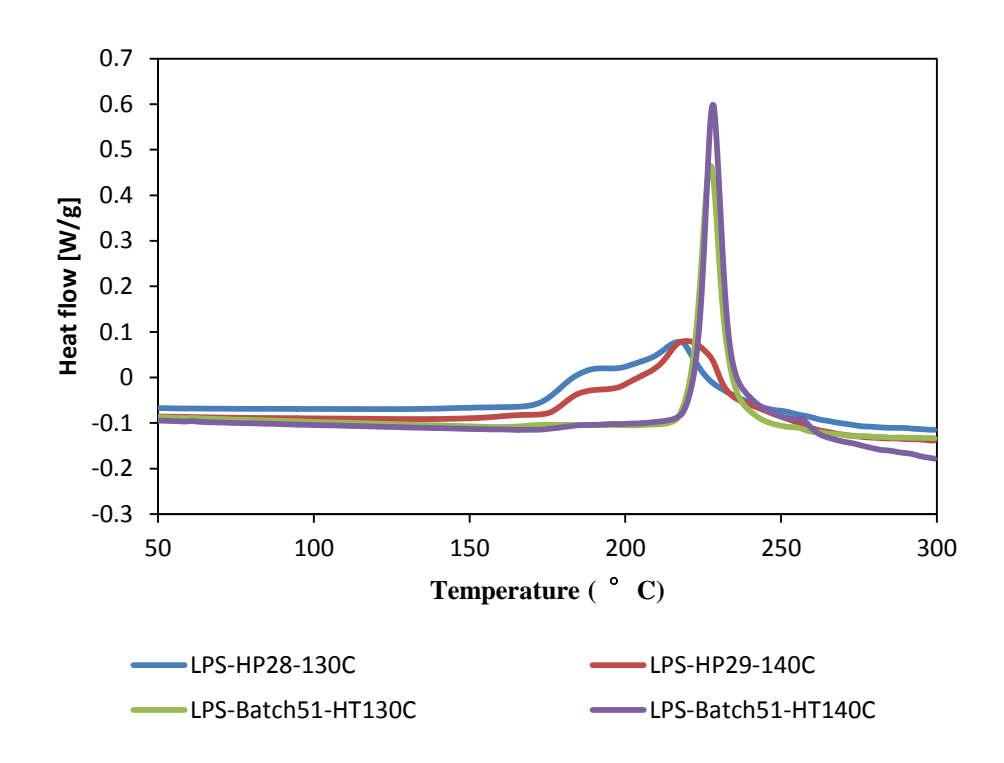


Figure 15. Effect of hot pressing at 130 and 140°C on DSC spectra of 75Li<sub>2</sub>S-25P<sub>2</sub>S<sub>5</sub>

From figure 14, it is shown that the DSC spectra changed after hot pressing it (HP-28-130C and HP-29-140C). Hot pressing not only broadens the temperature range in which the exothermic process takes place, but also the rate at which the energy is released is slower in comparison to the sharp peak (fast release of energy) seen in powders that were only thermally treated (no pressure during heating in the DSC). Both hot pressed pellets showed relatively the same profile even though the hot-pressed temperatures were 10°C apart. As discussed in more detail below, the additional exothermic peaks after hot pressing are likely consistent with partially crystallized LPS.

## 2.2.2. Evaluating the chemical and electrochemical stability of LPS

## 2.2.2.1. AC Impedance measurements and DC cycling

Different electrochemical tests were combined to characterize the stability of LPS during lithium cycling. Preconditioning was conducted (Fig. 15) on each of the pellets (data set no.1) to decrease the interfacial impedance between Li electrodes and LPS electrolyte. Moreover, AC impedance measurements are performed before and after every test to monitor the impedance of the electrolyte throughout the entire test.

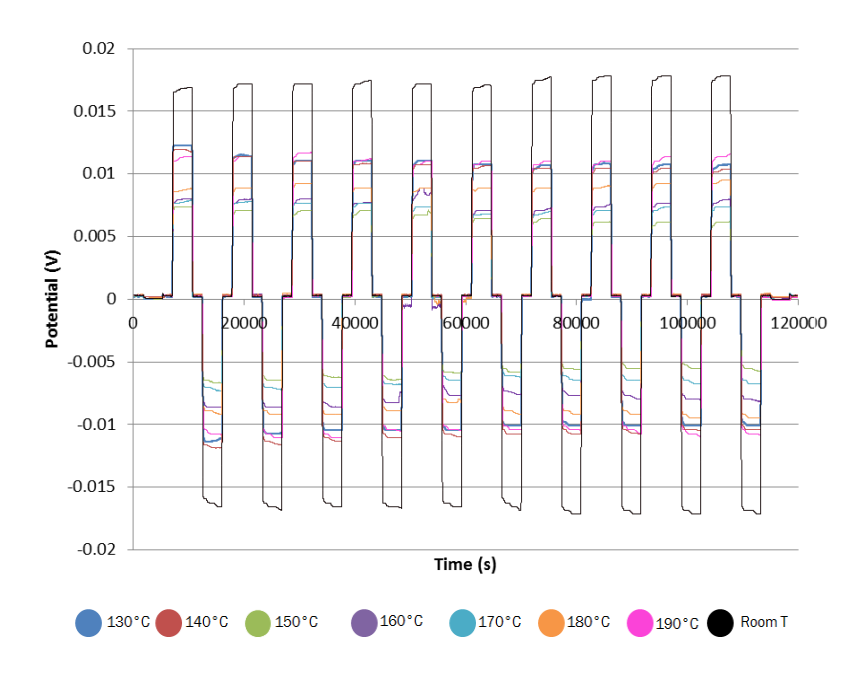


Figure 16. Li/75Li<sub>2</sub>S-25P<sub>2</sub>S<sub>5</sub>/Li cell preconditioning at room temperature,  $0.01~\text{mA/cm}^2$ 

For this data set, the polarizations in DC (Figure 15) agreed adequately with the cell impedances observed in AC (Figures 16 and 17), slightly above for the cold pressed pellet, and the hot-pressed samples at 180°C and 190°C. From Figure 15, it is clear that the cell with the pellet pressed at room temperature has the highest resistance, reflected as the highest polarization among samples.

Pressing temperature (°C)	Room temperature	130°C (HP-21)	140°C (HP-22)	150°C (HP-23)	160°C (HP-24)	170°C (HP-25)	180°C (HP-26)	190°C (HP-27)
Pellet area (cm <sup>2</sup> )	1.273	1.251	1.259	1.261	1.267	1.265	1.271	1.259
Pellet thickness (cm)	0.202	0.230	0.240	0.190	0.229	0.236	0.208	0.226
Area/thickness, A/l (cm)	6.32	5.44	5.26	6.62	5.53	5.37	6.12	5.58
75Li <sub>2</sub> S-25P <sub>2</sub> S <sub>5</sub> resistance (Ohm) - AC measurement before preconditioning	1091	897.88	876.34	484.76	557.98	498.36	589.46	661.58
Current (A)	1.27E-05	1.25E-05	1.26E-05	1.26E-05	1.27E-05	1.26E-05	1.27E-05	1.26E-05
V predicted (V)	0.014	0.011	0.011	0.006	0.007	0.006	0.007	0.008
V observed (V)	0.017	0.012	0.010	0.006	0.008	0.007	0.009	0.011

Table 4. Li/LPS/Li cell preconditioning at room temperature

The Nyquist plots before preconditioning (Figure 16 and 17) confirms through AC measurements that the cold-pressed pellet possess the highest resistivity to lithium transport in comparison to all the hot-pressed pellets, equal to 6900 Ohms\*cm. This might be an indicator that hot-pressing may change Li ionic transport. Moreover, the cell impedance decreased with increasing hot pressing temperature from 130°C to 170°C.

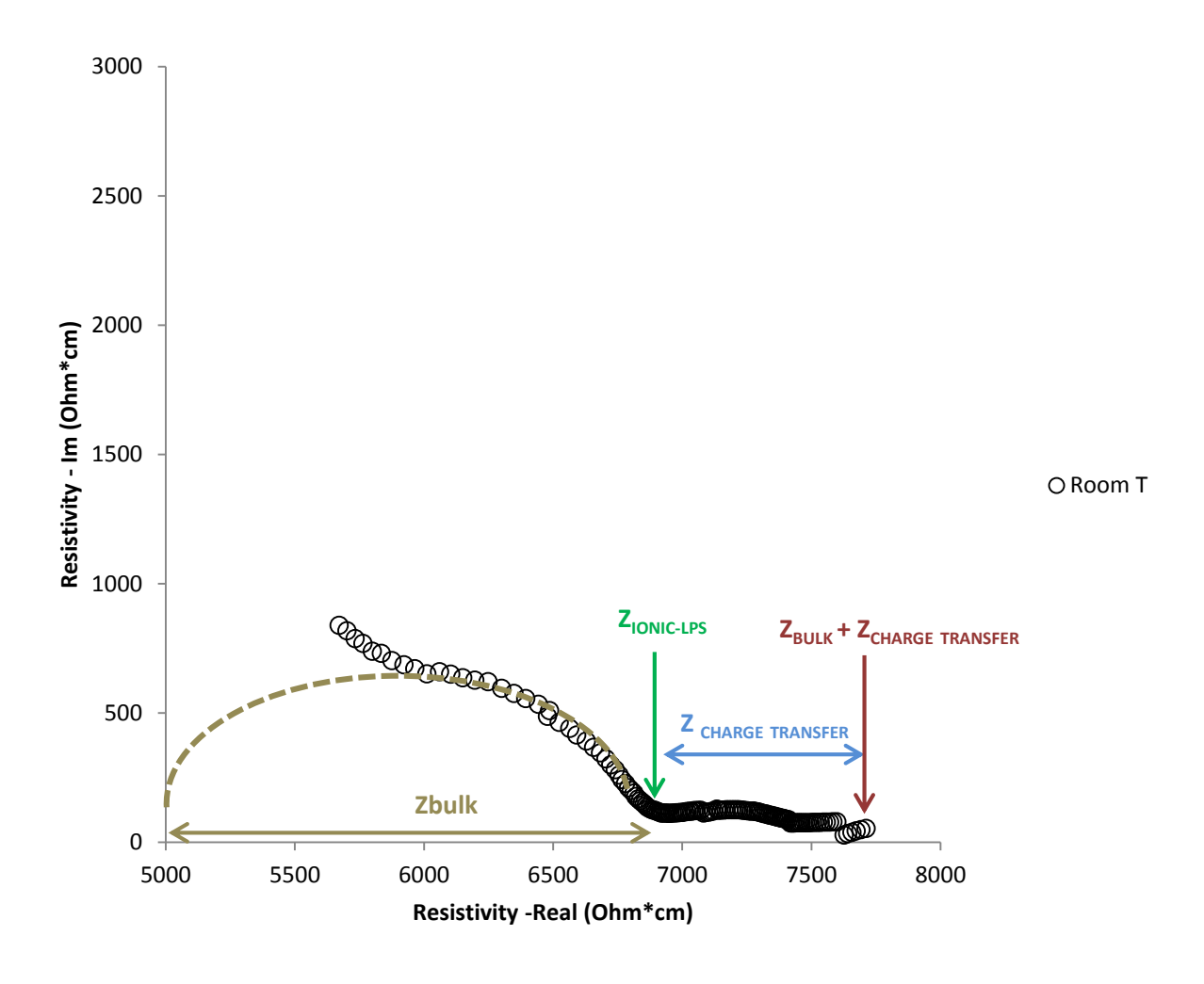


Figure 17. Nyquist plot of Li/LPS/Li cell before preconditioning at room temperature - Coldpressed pellet

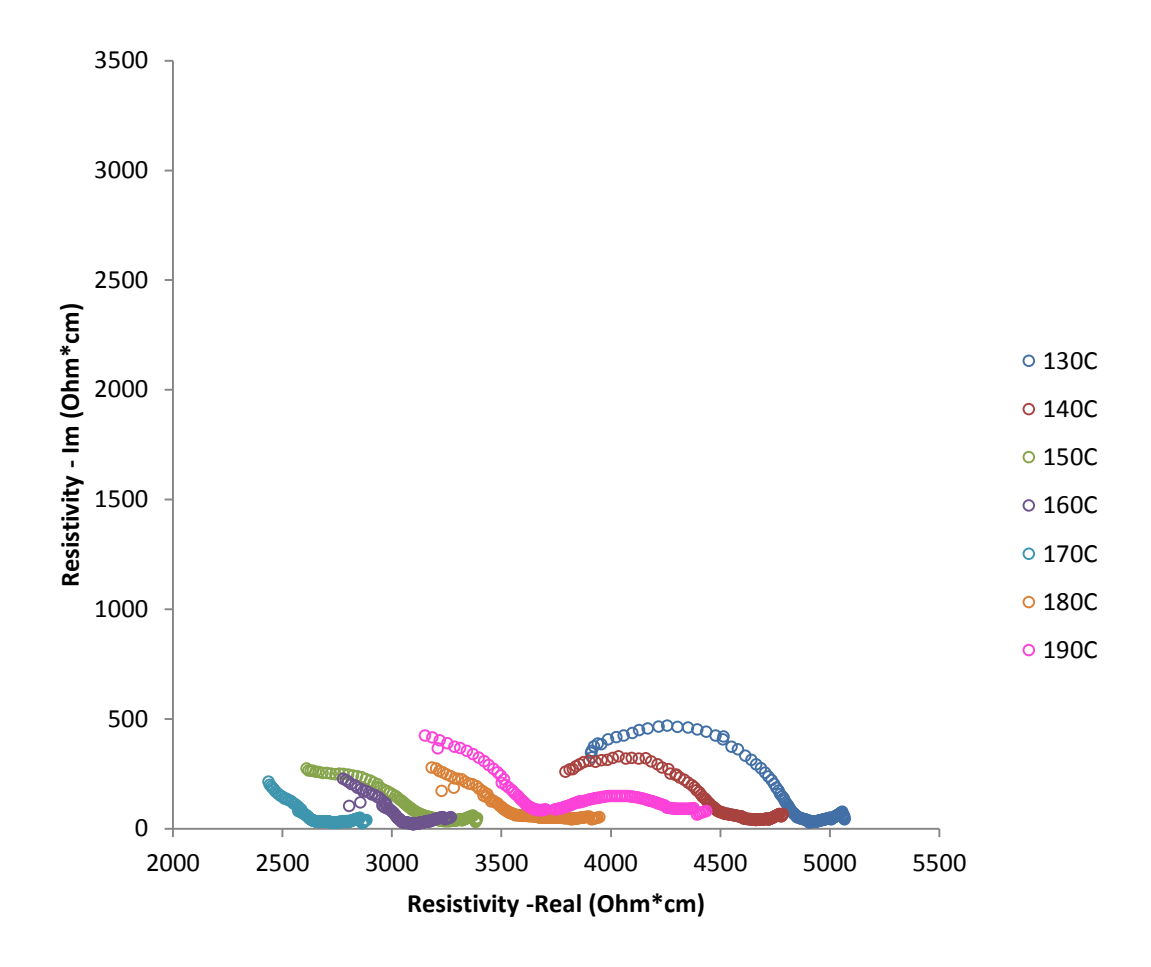


Figure 18. Nyquist plot of Li/LPS/Li cell before preconditioning at room temperature -Hot-pressed samples

After the preconditioning step (Figure 18 and 19), all samples showed a decrease in impedance as expected excluding the hot-pressed pellets at 180°C and 190°C and the cold-pressed pellet. This increase in resistance might be due to the formation of a resistive surface layer between the electrode and electrolyte. This would indicate chemical instability of the solid electrolyte against metallic lithium.

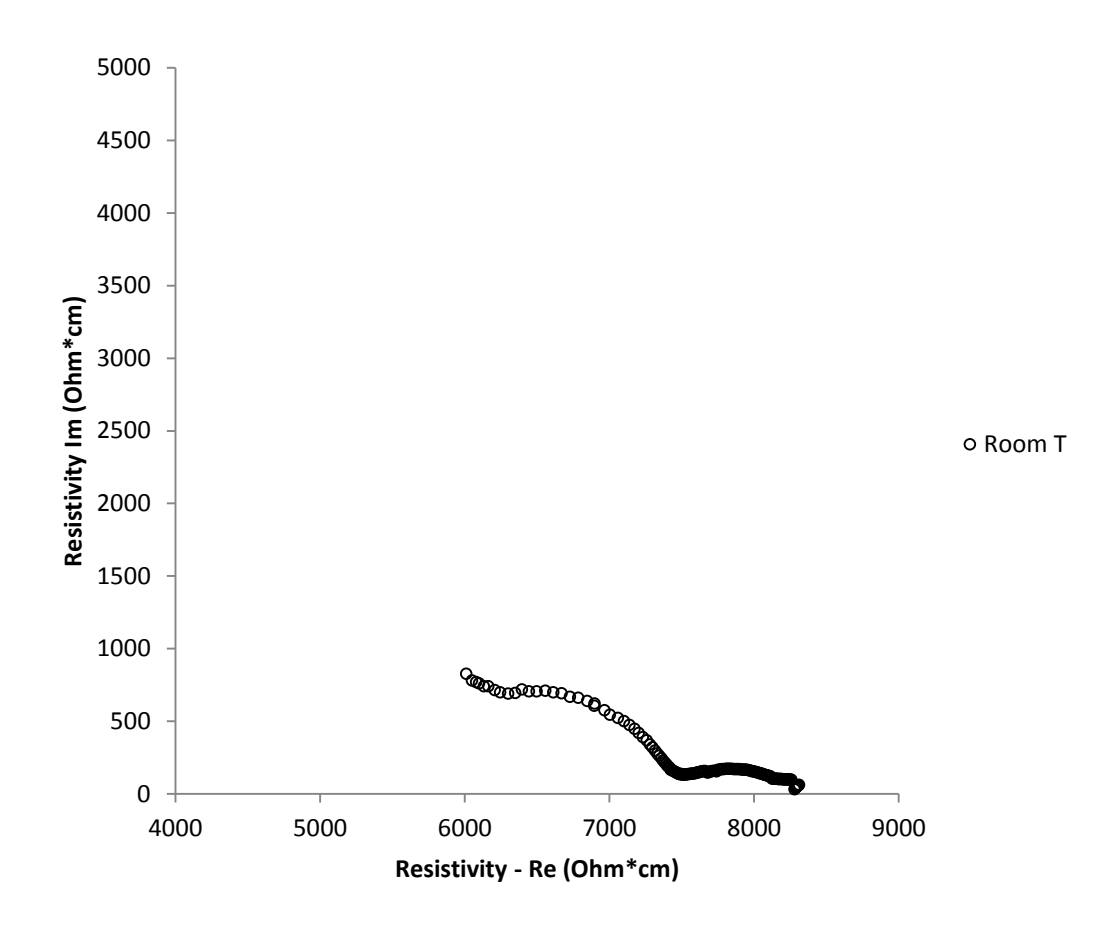


Figure 19. Nyquist plot of Li/LPS/Li cell after preconditioning at room temperature - Cold-pressed pellet

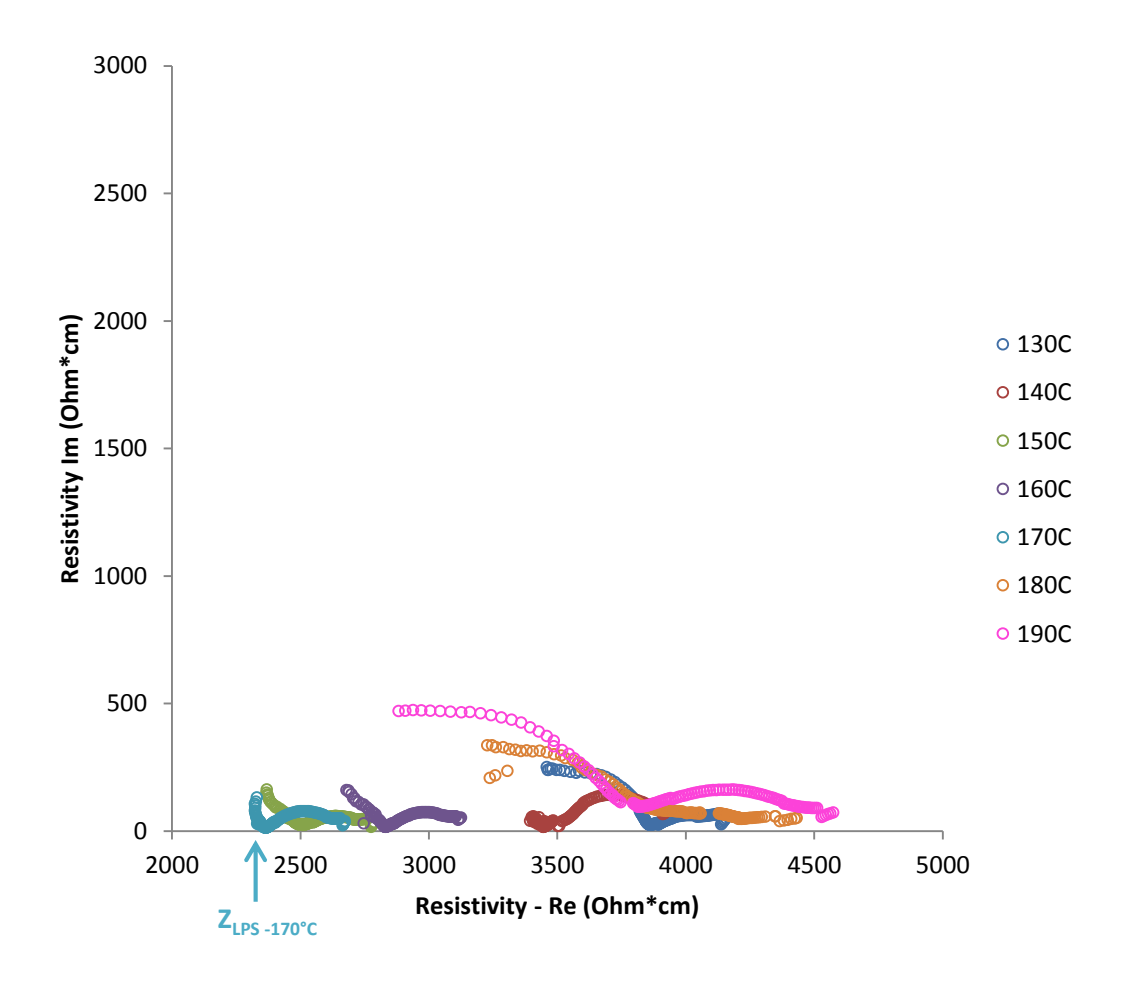


Figure 20. Nyquist plot of Li/LPS/Li cell after preconditioning at room temperature -Hot-pressed samples

The following figure is another representation of figures 18 and 19, but it points out more clearly that the pellets hot pressed at 150°C and 170°C had the lowest ionic impedances, especially 170°C equal to 2,344 Ohm\*cm, corresponding to an ionic conductivity of 0.4 mS/cm.

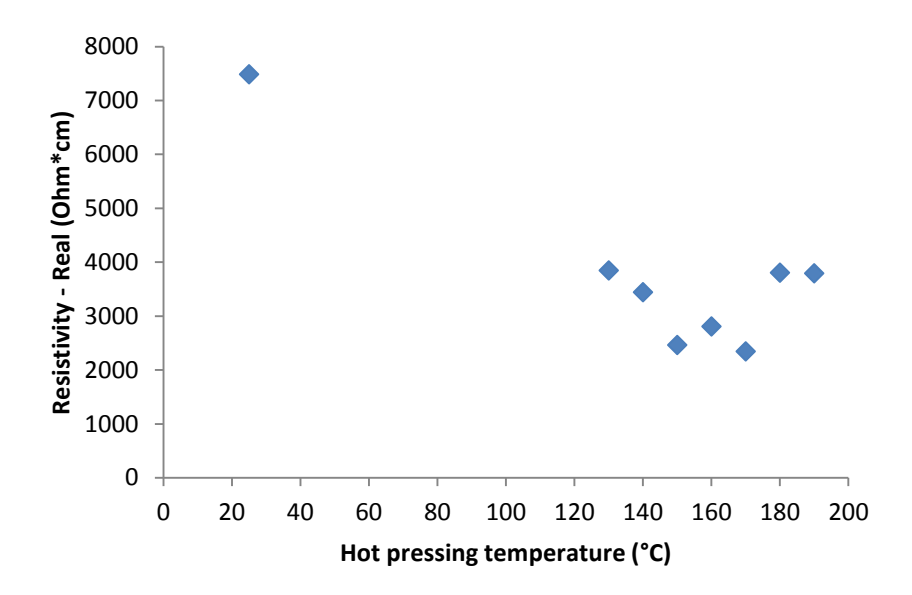


Figure 21. 75Li<sub>2</sub>S-25P<sub>2</sub>S<sub>5</sub> resistance (normalized by its aspect ratio) after preconditioning

After the preconditioning step was finished, a DC asymmetric polarization was conducted where lithium is passed through the Li/LPS/Li cell over a range of current densities. The idea of moving lithium in only one direction is to accurately identify (if any) the starting point where lithium penetrates and propagates through the electrolyte.

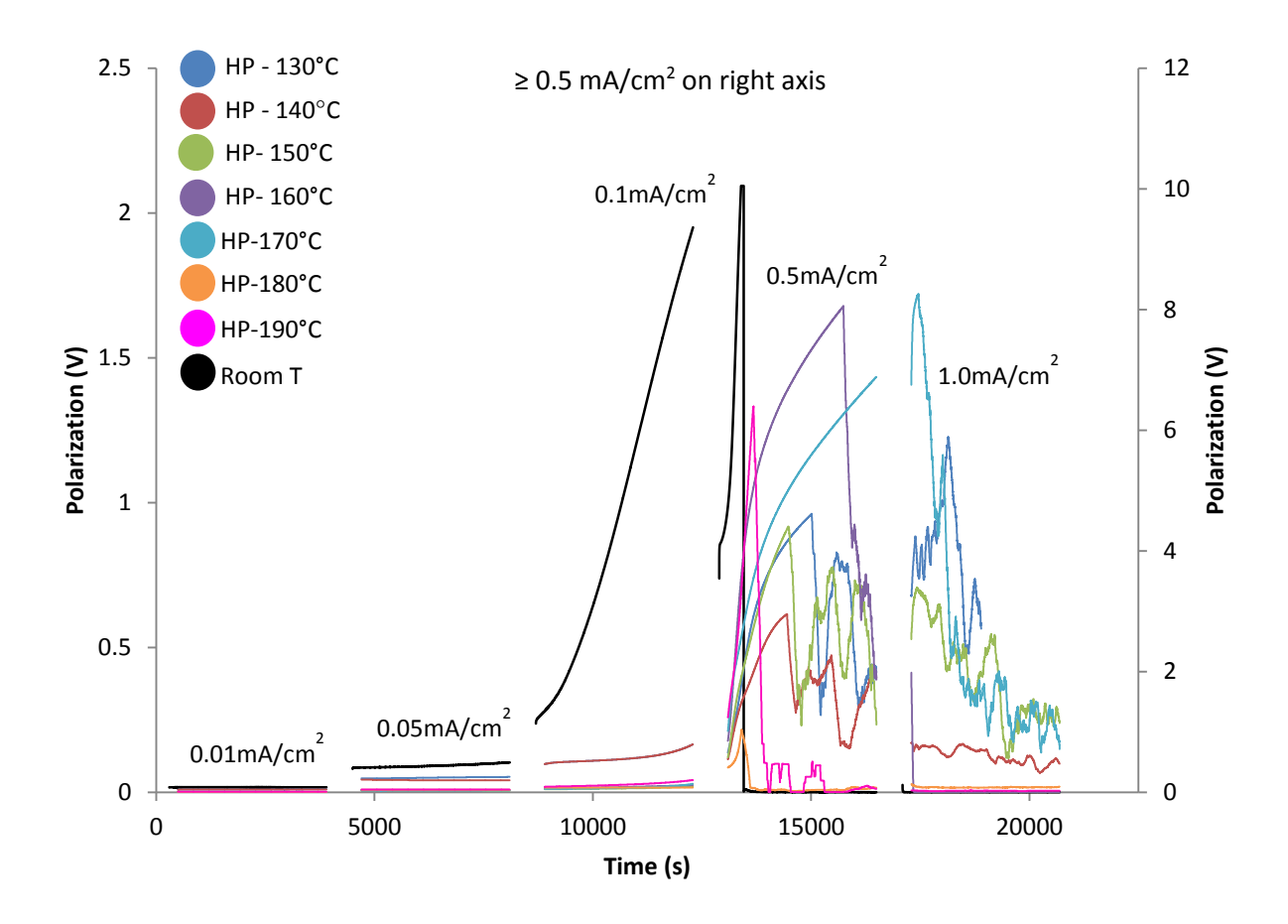


Figure 22. DC asymmetric polarization test at room temperature

For the first two current densities, 0.01 mA cm<sup>-2</sup> and 0.05 mA cm<sup>-2</sup> ohmic behavior was observed for all samples. At 0.1 mA cm<sup>-2</sup> a significant increase in polarization, thus an increase in resistance for the cold-pressed pellet is evident. At 0.5 mA cm<sup>-2</sup> all samples except for the one hot pressed at 170°C, the potential decreased significantly at some point within this current density. The decrease in potential is believed to be related to the formation of an electronically conducting phase that propagates between Li electrodes through the LPS; also referred to as a short circuit. Figure 22 markedly shows that the LPS powder hot-pressed at 170°C was the most electrochemically stable among this dataset. It was determined that 0.76 mA\*h cm<sup>-2</sup> of charged passed in order to decrease its potential from 8.63 V down to 0.99 V, i.e. cause the short circuit.

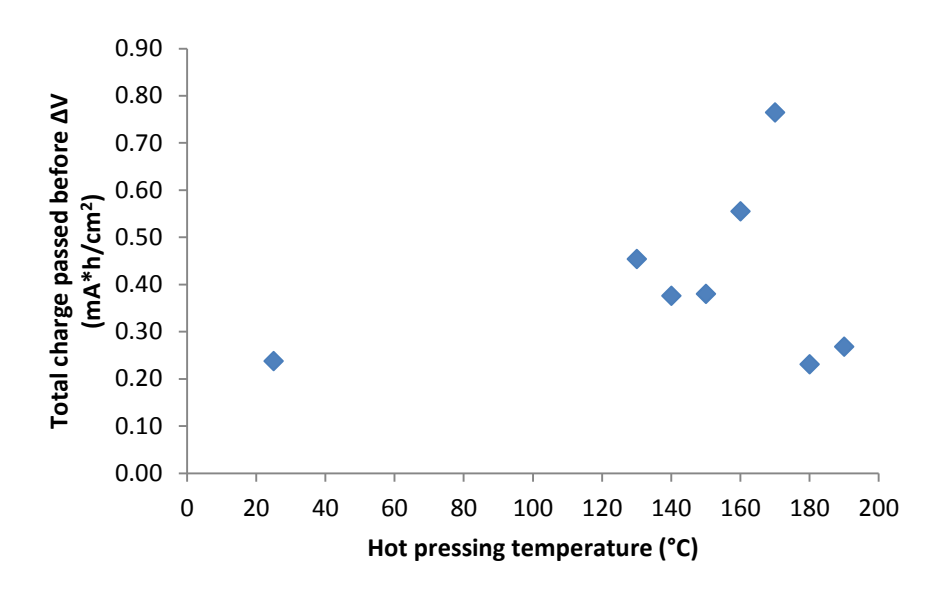


Figure 23. Total charge passed through Li/75Li<sub>2</sub>S-25P<sub>2</sub>S<sub>5</sub>/Li cell before significant drop in potential is observed in DC asymmetric polarization test

Additional evidence of short circuiting was observed in the AC measurements for the pellets hot pressed at 180°C and 190°C (HP-26 and HP-27). The lack of any capacitance (imaginary axis data) suggests that electronic conduction is the dominant transport mechanism as indicated in Figure 23. Additionally, negative imaginary data indicated inductance, which is also consistent with only electronic conduction.

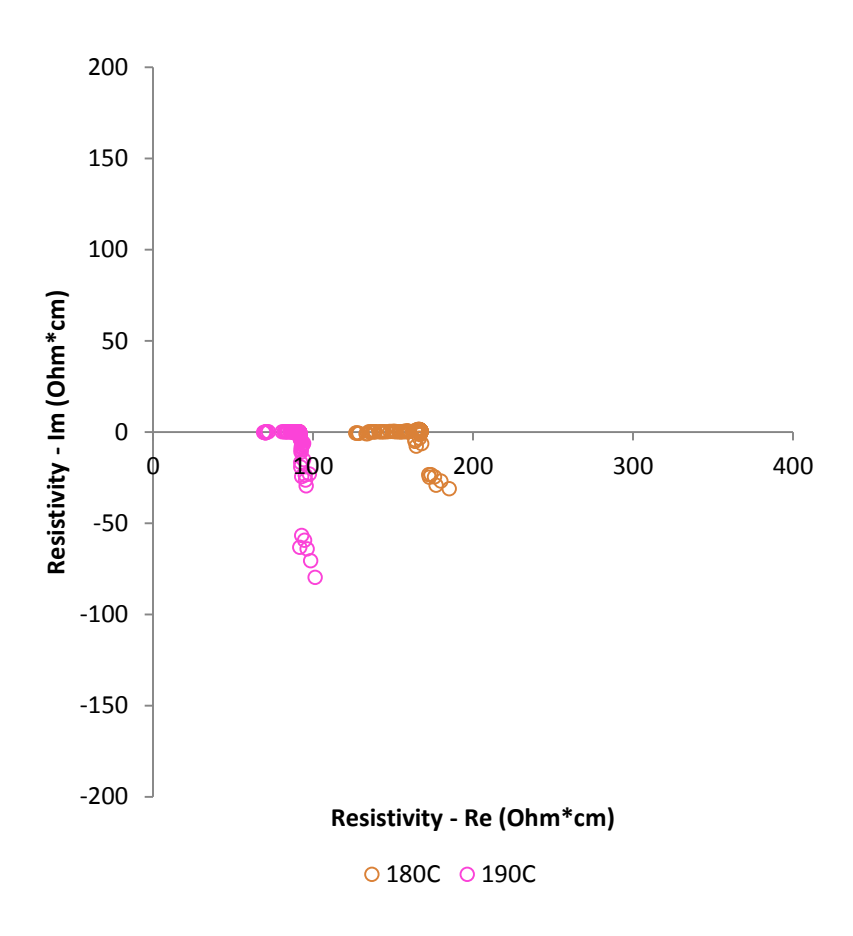


Figure 24. Nyquist plot of Li/LPS/Li cell after DC asymmetric polarization at room temperature – Hot-pressed pellets at 180°C and 190°C

# 2.2.2.2. Cross-sectional analysis

After the AC impedance measurements and DC cycling tests were completed, cross-sectional analysis was performed at MSU to identify the starting point where the electronically conductive phase initiates and propagates.

Pressing temperature	Plating side	Cross-section	Stripping side
Room temperature	12.7mm		
130°C			
140°C			
150°C			

Figure 25. Cross-sectional analysis on cold-pressed and hot-pressed pellets between 130°C and  $150^{\circ}\mathrm{C}$ 

Pressing temperature	Plating side	Cross-section	Stripping side
160°C			
170°C			
180°C			
190°C			

Figure 26. Cross-sectional analysis on cold-pressed and hot-pressed pellets between  $160^{\circ}\text{C}$  and  $190^{\circ}\text{C}$ 

All samples, except for the pellets hot-pressed at 140°C and 160°C, showed dendrite or decomposition phase penetration. Only the cold-pressed pellet and the pellets hot-pressed at 180°C and 190°C showed that the Lithium/decomposition phase started to propagate from the plating side going through the pellet until it reached the opposing electrode. Additionally, it was observed that the geometry of the penetration changed as the hot-press temperature increased. For example, the high-temperature pressed pellets (180°C and 190°C) shown a needle-shape penetration. Based on the DC asymmetric profiles, two different penetration mechanisms could be occurring. The first

mode of propagation can be represented by a sharp peak that decreases the voltage down to almost zero volts vs Li+/Li. The second mode of propagation can be represented by a voltage profile that decreases more gradually and with substantially more instability. The cold-pressed pellet and the high-temperature pressed pellets (180°C and 190°C) could be categorized into one group, all three showed a needle-shape penetration, a sharp peak was observed during the DC asymmetric test, and were the samples that showed the least discoloration. From this, it is suggested that in the absence of discoloration, the needle-shape penetration can be an indicator that an electronically conductive phase was the only phase that went through the pellet. However, in the other five samples, both the electronically conductive phase (believed to be lithium) and the decomposition phase (electronic insulator, ionic conductor) penetrated the pellet. The first phase was responsible of the voltage drop and the second phase what caused the instability in the voltage profile. Unfortunately, there are still many questions to be answered: why the decomposition phase is preferably formed in some pellets but not in others? Is it a contact issue related between the lithium electrode and the LPS electrolyte? Why the penetration occurs at certain locations but not in others? What makes one region of the pellet more likely to initiate the propagation of the decomposition reaction, i.e. what isn't the decomposition uniform across the pellet face? Further studies have to be performed to elucidate these phenomena. One approach is through materials characterization. Following XRD, DSC, SEM and EDS analyses before and after hot-pressing and DC cycling.

## 2.2.3. Materials characterization

## 2.2.3.1. X-Ray Diffraction Analysis

The XRD data showed that hot-pressing at and above 170°C, results in the formation of a crystalline phase (Figure 24). This suggests that the sample prepared was a glass-ceramic (Kingery,

1963). For the LPS system, glass-ceramics can show a higher ionic conductivity than their glass homologous, depending on which crystalline phase is precipitated from the mother glass. A highly conductive crystalline conductor like the thio-LISICON II analog would explain the decrease in resistance with increasing hot-pressing temperature trend observed in the AC measurements. However, due to the low peak intensity, the crystalline phase cannot be accurately identified. In contrast, the hot pressed pellet at 190°C with identifiable peaks at 17.5, 26, 27.5, 29 and 30, 2 theta correspond to the thio-LISICON III analog, which is not as conductive as thio-LISICON II analog. (Mizuno et al. 2006) Nevertheless, the increased conductivity with increasing hot pressing temperature suggests the formation of the relatively high conductivity crystalline thio-LISICON analogs compare to the LPS glass. (Mizuno et al. 2006)

The intensity of the XRD peaks decreased after the DC cycling was completed. This suggests that the long range atomic order obtained during hot pressing was disrupted by DC cycling reverting back to an amorphous phase.

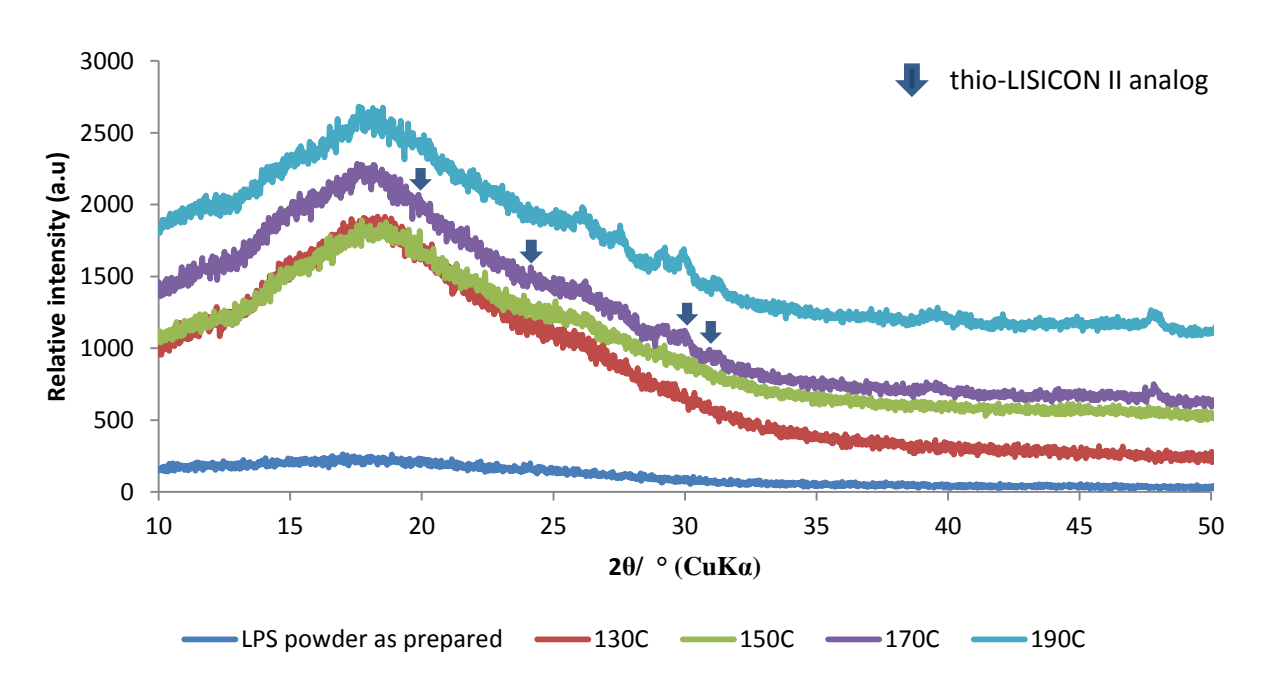


Figure 27. Effect of hot pressing temperature on 75Li<sub>2</sub>S-25P<sub>2</sub>S<sub>5</sub> structure

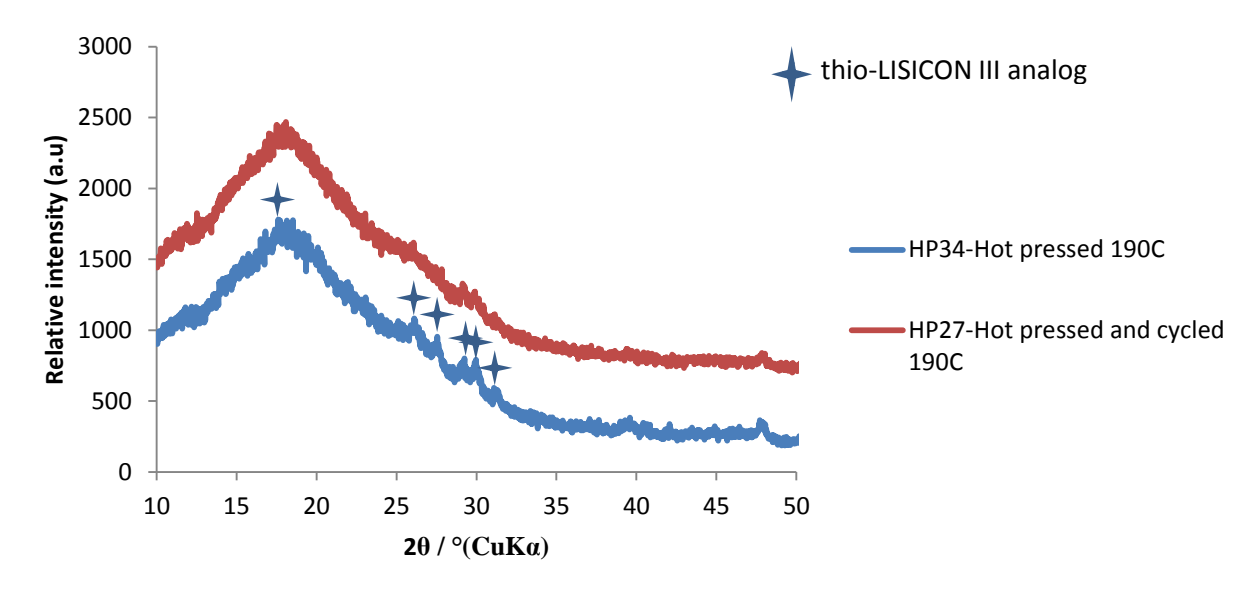


Figure 28. Effect of DC cycling on 75Li<sub>2</sub>S-25P<sub>2</sub>S<sub>5</sub> structure (hot pressed at 190°C)

# 2.2.3.2. Differential Scanning Calorimetry

DSC analysis showed that the exotherms present before DC asymmetric polarization (at approximately 190 and 220°C), disappeared after cycling suggesting that Li-ion transport through the LPS affects the bulk properties of the semi-crystallized LPS solid electrolyte. This may be an additional evidence of the transition from the crystalline phase precipitated during hot pressing back to an amorphous phase, which was detected by XRD.

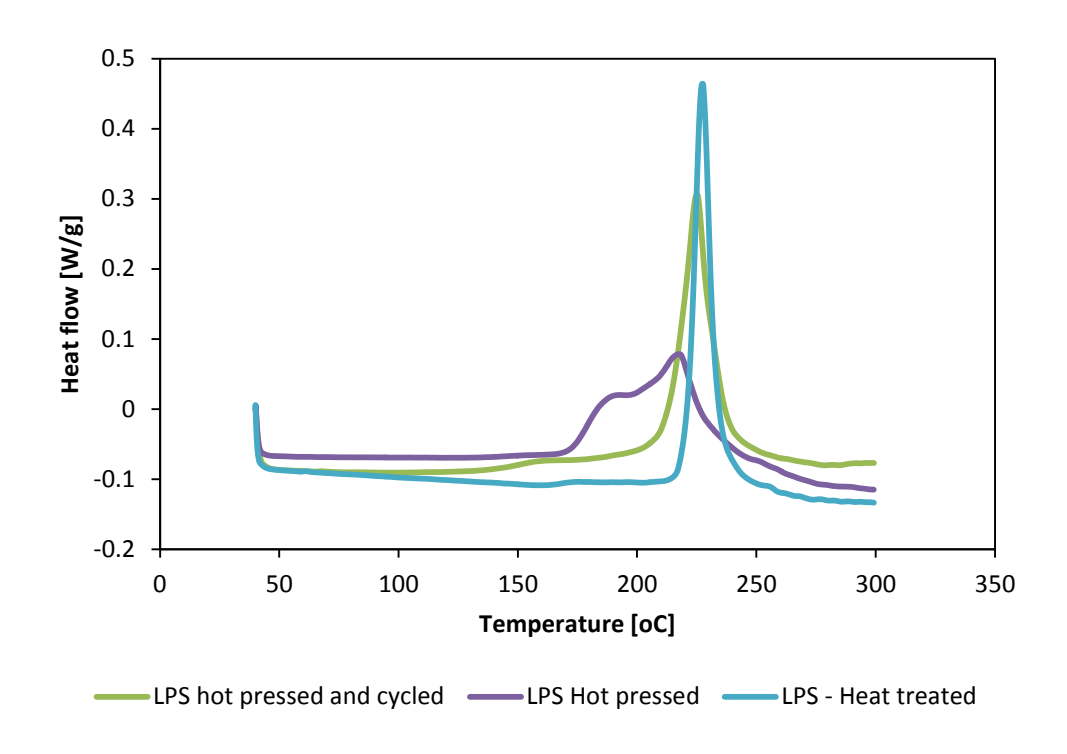


Figure 29. Effect of hot pressing and Li cycling on DSC spectra of  $75\text{Li}_2\text{S}-25\text{P}_2\text{S}_5$  hot-pressed at  $130^{\circ}\text{C}$ 

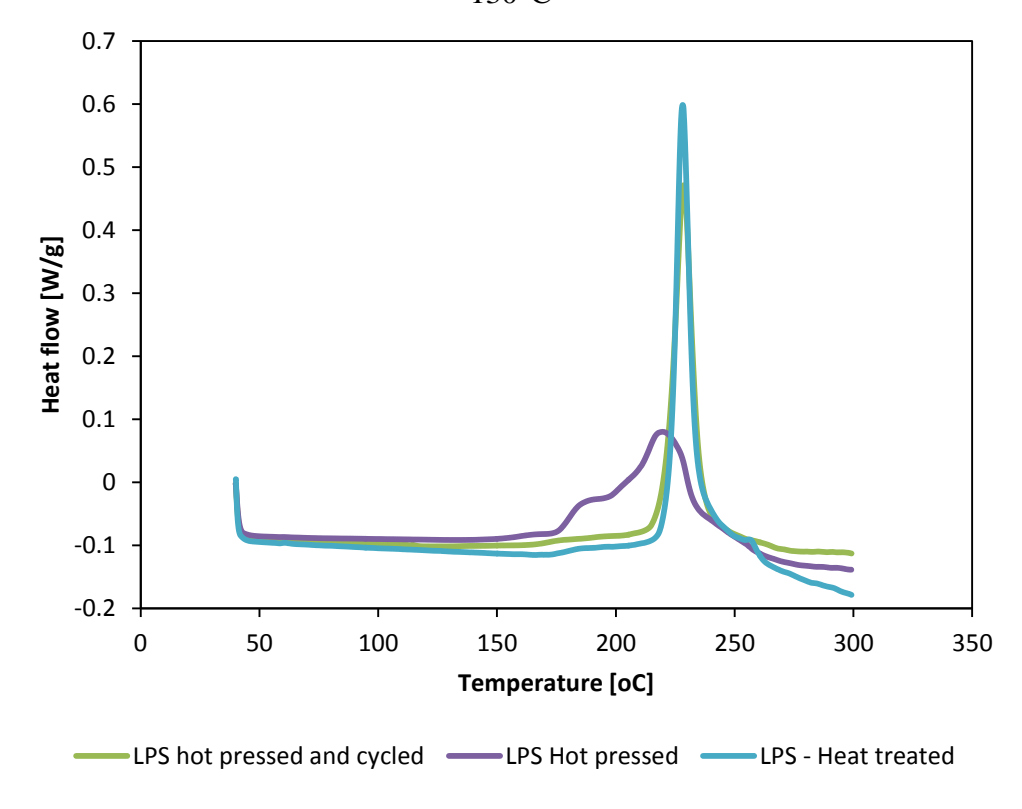


Figure 30. Effect of hot pressing and Li cycling on DSC spectra of  $75\text{Li}_2\text{S}-25\text{P}_2\text{S}_5$  hot-pressed at  $140^{\circ}\text{C}$ 

# 2.2.3.3. Scanning Electron Microscopy (SEM) and Energy Dispersive Spectrometry (EDS)

The morphology of the LPS after DC cycling did not change significantly as seen in the micrographs in Figure 28. The most noticeable feature was the increasing concentration of bright spots in the cycled pellets in comparison to the hot-pressed samples. Therefore, Energy Dispersive Spectrometry (EDS) was conducted to identify the composition of these areas. EDS showed that the bright particles detected in the hot-pressed and cycled pellets samples possess a higher concentration of sulfur than its surroundings. Moreover, these sulfur-rich particles could be the dark spots observed in the optical cross-sectional analysis, but this would not explain the drop in potential observed in the DC asymmetric tests. A surface analysis like X-ray photoelectron spectroscopy (XPS), sensitive to lithium is necessary to prove if lithium is propagating through the electrolyte.

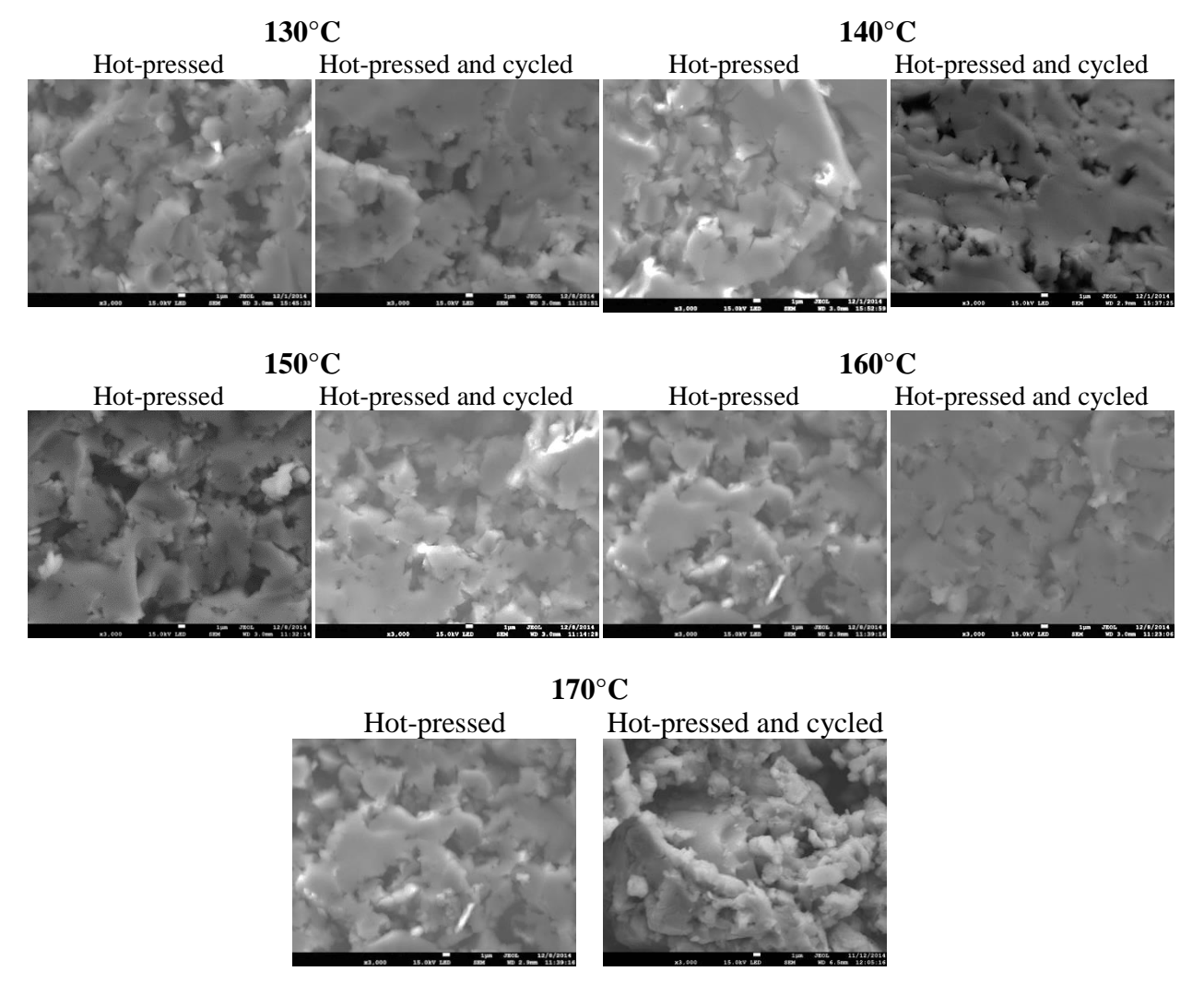


Figure 31. Fractured surfaces of hot pressed and DC cycled 75Li<sub>2</sub>S-25P<sub>2</sub>S<sub>5</sub> pellets

## 2.3. Conclusion

 $75\text{Li}_2\text{S}-25\text{P}_2\text{S}_5$  is a promising solid electrolyte owing to its attributes such as: high lithium ion conductivity ( $10^{-4}-10^{-3}$  S/cm) at room temperature and low cost constituents. Improving its utility for use in advanced, solid-state batteries, however, can be attained by improving its stability against metallic Li anodes. This work investigated hot-pressing as an approach to promote particle-particle chemistry thereby increasing stability. Increased conductivity was observed due to possible crystallization of a highly conductive phase during hot-pressing. However, the

crystallinity decreased as a result of the DC cycling. A clear correlation between processing conditions and density has not been elucidated, but it will be mandatory to increase its shear modulus, and ultimately avoid lithium dendrite penetration. The LPS system is versatile and demonstrates several of the key attributes necessary to enable solid-state batteries for electric vehicles or other applications.

### 2.4. Future directions

- Conduct density measurements via Archimedes method to verify densities calculated by geometrical methods.
- Perform conductivity measurements with ion-blocking electrodes for hot-press pellets at 150°C to 170°C (samples that showed least impedance among temperatures) to measure the ionic conductivity of LPS without no interaction with the electrodes.
- Identify the critical processing conditions necessary to control LPS porosity/density.
- Conduct EIS versus time measurements to characterize Li/LPS interface stability of the hot-press pellets at 150°C to 170°C.
- Perform Raman and XPS mapping analyses at cross-section and surfaces of cycled and only hot-pressed samples to accurately identify the phase migrating through the solid electrolyte.

REFERENCES

#### REFERENCES

- 1 Adachi, G.-Y., Imanaka, N., & Aono, H. (1996). Fast Li-Conducting Ceramic Electrolytes. Advanced Materials, 127–135.
- 2 H. Aono, E. Sugimoto, Y. Sadaoka, N. Imanaka, and G.-y. Adachi, *Chem. Lett.*, (1990) 331.
- 3 Bates, J. B., Dudney, N. J., Gruzalski, G. R., Zuhr, R. A., Choudhury, A., & Luck, C. F. (1993). Fabrication and characterization of amorphous lithium electrolyte thin films and rechargeable thin-film batteries. *Journal of Power Sources*, 43-44, 103–110.
- 4 Bruce, P.G., West, A.W. (1983). J. Electrochem Soc. 130(3), 662.
- 5 Brundle, C.R., Evans, C. A. Wilson, S. (1992). *Encyclopedia of Materials Characterization*. Gulf Professional Publishing. 751pp.
- 6 Burke, A. & Miller, M. (2011). Journal of Power Sources. *Journal of Power Sources*, 196(1), 514–522.
- 7 Callister, W. D. (2007). *Materials Science and Engineering, an Introduction*. John Wiley & Sons, Inc. 7<sup>th</sup> edition. 975pp.
- 8 Chu, Y. S. (2007). Basic Research Needs for Electrical Energy Storage: Report of the Basic Energy Sciences Workshop on Electrical Energy Storage. pp.1–186.
- 9 Chu, S. and Majumdar, A. (2012). *Nature*. Vol 488, 294-303.
- 10 C.W. Ban and G.M. Choi, Solid State Ionics, 140 (2001) 285.
- 11 Dunn, B., Kamath, H., & Tarascon, J. M. (2011). Electrical Energy Storage for the Grid: A Battery of Choices. *Science*, *334*(6058), 928–935. doi:10.1126/science.1212741
- 12 Etacheri, V. et al. *Energy Environ. Sci.* 4, 3243 (2011).
- 13 Hayashi, A., Hama, S., Morimoto, H., Tatsumisago, M., & Minami, T. (2001). Preparation of Li<sub>2</sub>S-P<sub>2</sub>S<sub>5</sub> Amorphous Solid Electrolytes by Mechanical milling. *Journal of the American Ceramic Society*, 84(2), 477–479.
- 14 Hayashi, A., Hama, S., Minami, T., Tatsumisago, M. (2003). Formation of superionic crystals from mechanically milled Li<sub>2</sub>S-P<sub>2</sub>S<sub>5</sub> glasses. *Electrochemistry Communications*, 5, 111-114.
- 15 Ho, C., Raistrick, I.D. and Huggins, R.A. J. Electrochem. Soc. 127, 343 (1980).

- 16 Hong, H. Y-P. (1978). Crystal structure and Ionic Conductivity of Li<sub>14</sub>Zn(GeO<sub>4</sub>)<sub>4</sub> and other new Li<sup>+</sup> superionic conductors.
- 17 Huggins, R. A. (2002). Simple Method to Determine Electronic and Ionic Components of the Conductivity in Mixed Conductors, A Review. *Ionics*, 8, 300–313.
- 18 Huggins, R. (2009). *Advanced Batteries: Materials Science Aspects*. United States of America. Springer.
- 19 H. Hyooma and K. Hayashi, *Mater. Res. Bull.*, 23 (1988) 1399.
- 20 Inaguma, Y., Chen, L., Itoh, M., Nakamura, T. (1994). Solid State Ionics. 70/71, 196.
- 21 Intergovernmental Panel on Climate Change. *Climate Change, Synthesis Report*. Edited by The Core Writing Team, Pachauri, R. K. and Meyer, L. http://www.ipcc.ch/pdf/assessment-report/ar5/syr/SYR\_AR5\_LONGERREPORT.pdf
- 22 International Energy Agency in World Energy Outlook (2011), 546-547 <a href="http://www.worldenergyoutlook.org">http://www.worldenergyoutlook.org</a> (International Energy Agency, 2011).
- 23 Irvine, J. T. S., Sinclair, D. C., & West, A. R. (1990). Electroceramics: Characterization by Impedance Spectroscopy. *Advanced Materials*, 2, 132–138.
- 24 Kanno, R and Murayama, M. (2001). *J. Electrochem. Soc.*, **148**, A742.
- 25 Kitaura, H., Hayashi, A., Ohtomo, T., Hama, S., & Tatsumisago, M. (2010). Fabrication of electrode–electrolyte interfaces in all-solid-state rechargeable lithium batteries by using a supercooled liquid state of the glassy electrolytes. *Journal of Materials Chemistry*, 21(1), 118. doi:10.1039/c0jm01090a
- 26 Knauth, P. (2009). Inorganic solid Li ion conductors: An overview. *Solid State Ionics*, *180*(14-16), 911–916. doi:10.1016/j.ssi.2009.03.022
- 27 Kingery, W.D., 1963. Effects of Applied Pressure on Densification during Sintering in the Presence of a Liquid. Journal of the American Ceramic Society, 46(8), pp.391–395.
- 28 Lee, R. (2011). Science. **333**, 569-573
- 29 L.O. Hagman and P. Kierkegaard, Acta Chem. Scand., 22 (1968) 1822.
- 30 M. Klingler, W.F. Chu, and W. Weppner, *Ionics*, 3 (1997) 289.
- 31 Minami, K. Mizuno, F. Hayashi, A., Tatsumisago, M. *Solid State Ionics*. 178 (2007), 837 841.
- 32 Mizuno, F. and Hayashi, A. (2005). New, Highly Ion-Conductive Crystals Precipitated from Li<sub>2</sub>S-P<sub>2</sub>S<sub>5</sub> glasses. *Advanced Materials*. 17(7), 918 921.
- 33 Mizuno, F.; Hayashi, A.; Tadanaga, K.; Tatsumisago, M. (2006). Solid State Ionics, 177, 2721.

- 34 Monroe, C., & Newman, J. (2005). The Impact of Elastic Deformation on Deposition Kinetics at Lithium/Polymer Interfaces. *Journal of the Electrochemical Society*, *152*(2), A396–A404. doi:10.1149/1.1850854
- 35 Morimoto, H., Yamashita, H., Tatsumisago, M. and Minami, T. (1999). Mechanochemical Synthesis of New Amorphous Materials of 60Li<sub>2</sub>S-40SiS<sub>2</sub> with high lithium ion conductivity. *J. Am. Ceram. Soc.* 82(5), 1352-1354.
- 36 Muramatsu, H., Hayashi, A., Ohtomo, T., Hama, S., Tatsumisago, M. (2011). Structural change of Li<sub>2</sub>S-P<sub>2</sub>S<sub>5</sub> sulfide solid electrolytes in the atmosphere. *Solid State Ionics*, 182, 116-119.
- 37 Murayama, M., Sonoyama, N., Yamada, A., Kanno, R. (2004). Solid State Ionics, 170, 173.
- 38 Murugan, R., Thangadurai, V. and Weppner, W. (2007). Angew. Chemie Inter. Ed.46, 7778.
- 39 Nazri, G.; Pistoia, G. *Lithium Batteries: Science and Technology*. United States of America. Springer.
- 40 Ohta, S. Kobayashi, T., Asaoka, T. (2011). High lithium ionic conductivity in the garnet-tupe oxide Li<sub>7-x</sub>La<sub>3</sub>(Za<sub>2-x</sub>, Nb<sub>x</sub>)O<sub>12</sub> (X = 0 -2). *Journal of Power Sources*. 196, 3342.
- 41 Ohtomo, T., Hayashi, A., Tatsumisago, M., Tsuchida, Y., Hama, S., & Kawamoto, K. (2013). Journal of Power Sources. *Journal of Power Sources*, 233(C), 231–235. doi:10.1016/j.jpowsour.2013.01.090
- 42 P.G Bruce, A.R. West. (1983). J. Electrochem. Soc. 30 662.
- 43 Sakamoto, J. (2014). *Handbook of Solid-State Batteries and Capacitors*. Chapter, Superionic conducting oxide electrolytes. Edited by N.J. Dudney, J. Nanda, and W. West. World Scientific Publishers.
- 44 Sakuda, A., Hayashi, A., & Tatsumisago, M. (2013). Sulfide Solid Electrolyte with Favorable Mechanical Property for All-Solid-State Lithium Battery. *Scientific Reports*, 3. doi:10.1038/srep02261
- 45 Sardela, M. (2014). Practical Materials Characterization. Springer. 237pp.
- 46 Sibilia, J. (1988). A Guide to Materials Characterization and Chemical Analysis. John Wiley & Sons. 408pp.
- 47 Song, M.-K., Zhang, Y. & Cairns, E.J., 2013. A Long-Life, High-Rate Lithium/Sulfur Cell: A Multifaceted Approach to Enhancing Cell Performance. 4.30.2014 Thesis Introduction\_Sections 1.5 1.7, 13(12), pp.5891–5899.
- 48 Stramare, S., Thangadurai, V., Weppner, W. (2003). Chem. Mater. 15, 3974.
- 49 Tachez, M., Malugani, J.P., Mercier, R., Robert, G. (1984). Solid State Ionics, 14, 181.

- 50 Takamasa, O., Hayashi, A., Tatsumisago, M. Tsuchida, Y., Hama, S., Kawamoto, K. (2013). All-solid-state lithium secondary batteries using the 75Li<sub>2</sub>S-25P<sub>2</sub>S<sub>5</sub> glass and the 70Li<sub>2</sub>S-30P<sub>2</sub>S<sub>5</sub> glass-ceramic as solid electrolytes. *Journal of Power Sources*, 233, 231-235.
- 51 Takeuchi, T., Kageyama, H., Nakanishi, K., Ohta, T., Sakuda, A., Sakaebe, H., Kobayashi, H., Tatsumi, K. and Ogumi, Z. Rapid preparation of Li<sub>2</sub>S-P<sub>2</sub>S<sub>5</sub> Solid Electrolyte and its application for Graphite/Li<sub>2</sub>S All-Solid-State Lithium Secondary Battery. *Electrochemistry Letters, ECS*. 3 (5), A31-A35. (2014).
- 52 Thackeray, M. M., Wolverton, C. and Isaacs, E. D. (2012). Energy Environ. Sci. 5, 7854.
- 53 Thompson, T., Wolfenstine, J., Allen, J. L., Johannes, M., Huq, A., David, I. N. and Sakamoto, J. (2014). Tetragonal vs. Cubic phase stability in Al-free Ta doped Li<sub>7</sub>La<sub>3</sub>Zr<sub>2</sub>O<sub>12</sub> (LLZO). *Journal of Materials Chemistry A.*, 2014, 2, 13431.
- 54 Virkar, A. V., Ketcham, T. D., & Gordon, R. S. (1979). Hot Pressing of Lithia-Stabilized IWAlumina. *Ceramurgia International*, 5(2), 66–69.
- 55 Wachsman, E. D., & Lee, K. T. (2011). Lowering the Temperature of Solid Oxide Fuel Cells. *Science*, *334*, 935–939. doi:10.1126/science.1212741
- 56 Wachtman, J., Cannon, W. R., Matthewson, M. J. (2009). *Mechanical properties of Ceramics*. John Wiley & Sons.